



**HAL**  
open science

# Comparison of existing strategies for keeping symmetrical peaks in on-line Hydrophilic Interaction Liquid Chromatography x Reversed-Phase Liquid Chromatography despite solvent strength mismatch

Soraya Chapel, Florent Rouvière, Sabine Heinisch

► **To cite this version:**

Soraya Chapel, Florent Rouvière, Sabine Heinisch. Comparison of existing strategies for keeping symmetrical peaks in on-line Hydrophilic Interaction Liquid Chromatography x Reversed-Phase Liquid Chromatography despite solvent strength mismatch. *Journal of Chromatography A*, 2021, 1642, pp.462001. 10.1016/j.chroma.2021.462001 . hal-03318522

**HAL Id: hal-03318522**

**<https://hal.science/hal-03318522>**

Submitted on 10 Mar 2023

**HAL** is a multi-disciplinary open access archive for the deposit and dissemination of scientific research documents, whether they are published or not. The documents may come from teaching and research institutions in France or abroad, or from public or private research centers.

L'archive ouverte pluridisciplinaire **HAL**, est destinée au dépôt et à la diffusion de documents scientifiques de niveau recherche, publiés ou non, émanant des établissements d'enseignement et de recherche français ou étrangers, des laboratoires publics ou privés.



Distributed under a Creative Commons Attribution - NonCommercial 4.0 International License

1 **Comparison of existing strategies for keeping symmetrical peaks in on-line Hydrophilic Interaction**  
2 **Liquid Chromatography x Reversed-Phase Liquid Chromatography despite solvent strength**  
3 **mismatch**

4

5 Soraya CHAPEL, Florent Rouvière, Sabine Heinisch\*

6

7 Université de Lyon, Institut des Sciences Analytiques, UMR 5280, CNRS, 5 rue de la Doua, 69100,

8 Villeurbanne, France

9

10

11 \*Corresponding author:

12 Sabine Heinisch

13 Tel: +33 437 423 551

14 E-mail address: [sabine.heinisch@univ-lyon1.fr](mailto:sabine.heinisch@univ-lyon1.fr)

15

16

17 **ABSTRACT**

18 In two-dimensional liquid chromatography, the combination of hydrophilic interaction liquid  
19 chromatography (HILIC) and reversed-phase liquid chromatography (RPLC) is very attractive due to  
20 the complementarity of their separation mechanisms. On-line comprehensive HILIC x RPLC is well-  
21 known to give rise to a large retention space coverage when dealing with ionisable compounds.  
22 However, method development in on-line HILIC x RPLC is challenging due to the reversed solvent  
23 strength between both dimensions, which can greatly affect the peak shapes in the second RPLC  
24 dimension and thus the separation quality and the method sensitivity. In the present contribution,  
25 we compared four strategies designed to avoid this problem: (1) flow splitting, which consists in  
26 reducing the injection volume in the second dimension (<sup>2</sup>D), (2) on-line dilution with a make-up flow  
27 and (3) on-line dilution with Active Solvent Modulation (ASM), which both consist in reducing the  
28 solvent strength of the injected fractions, and (4) Total Breakthrough Strategy which we recently  
29 proposed. Unlike the three preceding strategies, this latter one consists in injecting large volumes of  
30 strong solvent in <sup>2</sup>D. The performance of each strategy was evaluated for sub-hour separations of a  
31 tryptic digest in on-line HILIC x RPLC. In this work, we considered the critical case for which the same  
32 column internal diameters (i.e. 2.1 mm here) are used in both dimensions. Peak capacity, peak  
33 shapes and peak intensities were considered for this evaluation. The highest peak capacity could be  
34 achieved with Total Breakthrough Strategy while the lowest one with on-line dilution using ASM.  
35 Peak intensities were usually higher with on-line dilution approaches (make-up flow and ASM).

36 However, despite the presence of breakthrough, peak intensities were approximately 7-fold higher  
37 with Total Breakthrough Strategy than with flow splitting.

38

### 39 **Keywords**

40 Two-dimensional liquid chromatography; on-line HILIC x RPLC; solvent strength mismatch; tryptic  
41 digest; breakthrough phenomenon

42

### 43 **1. Introduction**

44

45 On-line comprehensive two-dimensional liquid chromatography (LC x LC) is a powerful tool to deal  
46 with highly complex samples. The potential of this technique has been highlighted in various  
47 application areas, including, among the most recent ones, proteomics [1], metabolomics [2], natural  
48 product research [3], polymer analysis [4], and pharmaceutical analysis [5]. The basic principle of  
49 two-dimensional liquid chromatography (2D-LC) is the combination of two chromatographic  
50 systems, referred to as dimensions, to expand the level of information on a given sample. To be  
51 effective, the two dimensions must provide different selectivities. This is usually achieved by  
52 selecting two chromatographic modes with different retention mechanisms. In on-line  
53 comprehensive 2D-LC (on-line LC x LC), the entire effluent from the first dimension (<sup>1</sup>D) is  
54 fractionated and continuously transferred to the second dimension (<sup>2</sup>D) through a switching-valve,  
55 often referred to as modulator. Compared to conventional one-dimensional liquid chromatography  
56 (1D-LC), a drastic improvement of the resolving power is expected. In theory, the peak capacity  
57 should be the product of the peak capacities in the two dimensions. In practice, this is true if the <sup>1</sup>D-  
58 separation is preserved and if the available 2D separation space is fully occupied by peaks (i.e. if the  
59 two separation dimensions are fully orthogonal). Apart from a few lucky combinations, such as HIC x  
60 RPLC [6], HIC x SEC [7] or IEX x RPLC [8], for which the mobile phase in <sup>1</sup>D becomes a weak injection  
61 solvent in <sup>2</sup>D, the quest for a higher degree of orthogonality between the two dimensions often  
62 leads to a decreased compatibility between the mobile phase in <sup>1</sup>D and the separation in <sup>2</sup>D.

63 A typical example of this duality is the combination of hydrophilic interaction liquid chromatography  
64 (HILIC) and reversed-phase liquid chromatography (RPLC). In the past decade, HILIC x RPLC has  
65 received a substantial increase in interest for the on-line LC x LC separation of polar and ionisable  
66 compounds [9–12]. This growing popularity is driven by the complementarity of the two separation  
67 mechanisms which gives rise to high coverage of the two-dimensional retention space [2,13].  
68 However, due to the opposite eluent strengths of the two mobile phases, on-line HILIC x RPLC is not  
69 guaranteed to succeed. The mobile phase in HILIC typically contains a high percentage of acetonitrile

70 (i.e. > 50%) which is a strong eluent in RPLC. The transfer of acetonitrile-rich fractions from <sup>1</sup>D-HILIC  
71 usually greatly impacts the peak shapes in <sup>2</sup>D-RPLC, the solute band being not or partly retained in  
72 the <sup>2</sup>D column. This may lead to band broadening, peak distortion, and/or analyte breakthrough.  
73 Breakthrough is a phenomenon that occurs when part of the sample migrates through the column  
74 without any retention and elute with the solvent peak whereas the other part undergoes normal  
75 retention, which results in the presence of an unretained peak in addition to the expected retained  
76 peak. The shape of the retained peak depends on (1) the solute retention in the injection solvent, (2)  
77 the solute retention in the mobile phase, and (3) the injection volume. These injection effects  
78 negatively impact the separation in <sup>2</sup>D by decreasing both the peak capacity and the peak intensity.  
79 Solvent strength mismatch is by far the most critical reported issue in on-line HILIC x RPLC [2,3,14–  
80 16]. To overcome its deleterious impact on the separation in <sup>2</sup>D, a few strategies were proposed  
81 over the years. They fall into two broad categories: (i) reducing the injection volume or (ii) reducing  
82 the eluent strength of the injection solvent by on-line dilution with a weak solvent. Reducing the  
83 volume injected in <sup>2</sup>D can be achieved either by selecting appropriate column internal diameters in  
84 each dimension [9] (usually at least twice as large in <sup>2</sup>D) or more commonly by splitting the flow  
85 coming from <sup>1</sup>D with a tee-piece and appropriate tubing [17]. Both approaches inevitably result in  
86 increased dilution. On-line solvent dilution consists in diluting the <sup>1</sup>D organic-rich fractions with  
87 water before injection in <sup>2</sup>D. Three different methods were reported. The most widespread one  
88 makes use of a make-up pump between the <sup>1</sup>D-column and the interface valve [18]. The flow rate  
89 delivered by the pump can be varied depending on the desired dilution. In 2017, a new valve  
90 permitting to achieve dilution inside the valve using restriction capillaries was introduced. It was  
91 referred to as “Active Solvent Modulation” (ASM) [19,20]. More recently, the so-called “At-Column  
92 Dilution” (ACD) was proposed. In this case, dilution is carried out between the valve and the <sup>2</sup>D-  
93 column by using an additional pump to empty the sample loop while the <sup>2</sup>D-pump dilutes the  
94 transferred fractions [21,22]. Regardless of the method, very large volumes which are proportional  
95 to the desired dilution ratio, are injected in <sup>2</sup>D. Nevertheless, improvements in both peak shape and  
96 peak intensity can be expected from the substantial decrease in eluent strength, which promotes  
97 band focusing at the <sup>2</sup>D-column inlet. It should be noted that despite the decrease in solvent  
98 strength, very large injection volumes can still have a detrimental effect on peak shapes, especially  
99 for less retained compounds. This was highlighted in the context of the separation of  
100 pharmaceuticals in 1D-LC [23]. The combination of both on-line dilution and flow splitting was  
101 suggested to lessen this problem [11,23] but this approach was not compared to on-line dilution  
102 alone. Similarly, the use of short trap columns instead of conventional empty loops after on-line  
103 dilution with a make-up flow was subjected to numerous developments in recent years [24]. Trap

104 columns are supposed to reduce the injection volume after on-line dilution by trapping the analytes  
105 before being sent to the 2D column. Despite the increased popularity of trap columns in on-line HILIC  
106 x RPLC [10,12,25,26], their added value in combination with on-line dilution has still to be  
107 demonstrated. Furthermore, the use of 2D-methods with trap columns is questionable for routine  
108 analysis since it is more difficult to develop and less rugged considering the risk of sample loss and  
109 incomplete recovery.

110 In a previous work [13], we presented an alternative approach for the separation of peptides in on-  
111 line HILIC x RPLC that we called "Total Breakthrough Strategy" (TBS). This approach relies on the  
112 injection of relatively large volumes of strong solvent without flow-splitting and on-line dilution.  
113 Unlike the above strategies, for which breakthrough is unwelcome, our approach is supported by the  
114 existence of breakthrough. For large enough injection volumes, it was shown that quite symmetrical  
115 peaks could be obtained in 2D-RPLC. It was also proved that the peak retention time exactly matches  
116 the one obtained by injecting a small analyte volume in a weak solvent. Furthermore, despite the  
117 presence of breakthrough, quantitative analysis on the retained peak was proved to be quite  
118 reliable. Such conclusions could be drawn provided that the injected volume was above a specific  
119 critical volume which depends on the analyte, its retention, and its injection solvent [13]. In this  
120 case, the area of the retained peak varies linearly with the injected amount which is not the case at  
121 an earlier stage of breakthrough (i.e. below the critical volume). The validity of this approach in on-  
122 line HILIC x RPLC was demonstrated under a broad range of conditions in the context of peptide  
123 analysis.

124 The aim of the present study was to compare four of the above-cited strategies, designed to  
125 overcome solvent strength mismatch in on-line HILIC x RPLC. In this work, we have considered the  
126 critical case for which the same column internal diameter (here 2.1 mm) is used in both dimensions.  
127 The compared strategies include (i) the Total Breakthrough strategy (TBS) [13], (ii) the flow splitting  
128 strategy (FSS), (iii) the make-up flow strategy (MFS), and (iv) the active solvent modulation strategy  
129 (ASMS). Their strengths and weaknesses are identified in the context of an optimized sub-hour  
130 separation of a tryptic digest in on-line HILIC x RPLC with a view to select the most appropriate one.

131

## 132 **2. Experimental section**

### 133 2.1. Chemicals and reagents

134

135 Acetonitrile (ACN, LC-MS grade) was obtained from Sigma-Aldrich (Steinheim, Germany). Water was  
136 purified and deionized in-house using an Elga Purelab Classic UV purification system from Veolia  
137 water STI (Décines-charpieu, France). Formic acid (FA, LC-MS grade), ammonium acetate, and

138 ammonium bicarbonate (both analytical reagent grade) were obtained from Fischer scientific  
139 (Illkirch, France). DL-1,4-dithiothreitol (DTT, 99%) and iodoacetamide (98%) were obtained from  
140 Acros Organics (Geel, Belgium). Trypsin, human serum albumin (HSA), bovine serum albumin (BSA),  
141  $\beta$ -casein, myoglobin, lysozyme, and cytochrome C were all obtained from Sigma-Aldrich (Steinheim,  
142 Germany).

143

## 144 2.2. Sample preparation

145

146 A model sample was obtained by tryptic digestion of six proteins (HSA, BSA,  $\beta$ -casein, myoglobin,  
147 lysozyme, and cytochrome C) following a protocol described elsewhere [13,17].

148 The aqueous digests were 2-fold diluted with ACN and filtered on 0.22  $\mu$ m PVDF (polyvinylidene  
149 fluoride) membranes before injection in <sup>1</sup>D-HILIC.

150

## 151 2.3. Instrumentation

152

153 2D-LC experiments were carried out on a 1290 series Infinity 2D-LC system from Agilent  
154 Technologies (Waldbronn, Germany). The system includes two high-pressure binary pumps, a  
155 thermostated autosampler with a flow-through needle injector, two thermostated column  
156 compartments with low-dispersion preheaters, and two diode-array UV absorbance detectors (DAD)  
157 with 0.6  $\mu$ L flow-cells. The switching-valve connecting the two dimensions was either a 2-position /4-  
158 port duo valve (Fig. S1) or a 4-position/10-port Active Solvent Modulation (ASM) valve (Fig. S2), both  
159 configured in backflush mode to minimize extra-column dispersion. In this paper, the first one will be  
160 referred to as a standard valve, the second one as the ASM-valve. Depending on the transferred  
161 fraction volume, the valves were equipped with two identical sample loops of either 20  $\mu$ L (0.2 mm  
162 ID), 40  $\mu$ L (0.25 mm ID for the standard valve, and 0.35 mm ID for the ASM valve) or 180  $\mu$ L (0.35  
163 mm ID). For on-line dilution, the sample loops were connected to the valve through two parking  
164 deck (valves used for multiple heart-cutting 2D-LC) using two transfer capillaries of 1.9  $\mu$ L (0.35 mm  
165 ID). A schematic representation of this configuration is shown in Fig. S3. For the make-up flow  
166 approach, this setup was used to circumvent the incompatibility of the commercialized 180  $\mu$ L loops  
167 fitting with the standard valve ports. In the case of ASM, not only the comprehensive 2D-LC sample  
168 loops are not compatible with the ports of the ASM valve, but this technique also requires  
169 backpressure from capillaries between the ASM valve and the multiple heart-cutting valves to  
170 function. A pressure release kit was installed between the <sup>1</sup>D outlet and the modulation valve inlet  
171 to minimize baseline disturbances coming from 2D-LC valve switching. The dwell volumes and extra-

172 column volumes were respectively 170  $\mu\text{L}$  and 22  $\mu\text{L}$  in  $^1\text{D}$ , and 80  $\mu\text{L}$  and 8.5  $\mu\text{L}$  in  $^2\text{D}$  (loop volume  
173 excluded). For the make-up flow strategy, an additional high-pressure binary pump from an Acquity  
174 UPLC I-Class liquid chromatography system from Waters (Milford, MA, USA) was used. The  
175 schematic representations of the four different setups used in this work are given in Fig.1.

176 The 2D-LC system was hyphenated to an Agilent Q-TOF mass spectrometer (model G6545B)  
177 equipped with a Jet Stream electrospray ionization (ESI) source. The 2D-LC-UV system and the  
178 additional high-pressure pump were controlled using Agilent OpenLab software and Waters  
179 MassLynx software, respectively. The mass spectrometer was controlled using Agilent MassHunter  
180 software. The HRMS data were processed using Agilent MassHunter qualitative analysis software.

181

#### 182 2.4. Chromatographic and detection conditions

183

184 For a fair comparison, similar conditions were used for the four presented strategies. The conditions  
185 were optimized in a previous study dealing with the on-line HILIC x RPLC separation of peptides in 30  
186 min [13]. The  $^1\text{D}$ -HILIC separation was performed using an Acquity BEH HILIC column (50 x 2.1mm;  
187 1.7  $\mu\text{m}$  particles) from Waters (Milford, MA, USA). The column temperature was set at 30°C and the  
188 flow rate was 0.05 mL/min. The injected volume was 6  $\mu\text{L}$ . A gradient elution with ACN as solvent A  
189 and 10 mM ammonium acetate in water as solvent B (pH of 6.8 in the aqueous phase) was carried  
190 out as follows: 0 min (2% B), 30 min (52% B), 32.4 min (2% B), and 50 min (2% B). UV chromatograms  
191 were recorded at 210 nm with an acquisition rate of 20 Hz. The sampling time was 0.39 min.  
192 Depending on the studied strategy, the transferred fractions were modified or not before injection  
193 in  $^2\text{D}$  as discussed in the next section.

194 The  $^2\text{D}$ -RPLC separation was performed using an Acquity CSH C18 column (30 x 2.1 mm; 1.7  $\mu\text{m}$   
195 particles) from Waters (Milford, MA, USA). The column temperature was set at 80°C and the flow  
196 rate was 2 mL/min. Water was used as solvent A and ACN as solvent B, both with 0.1% formic acid  
197 (pH = 2.7). Initial and final compositions were 1% B and 45% B. The gradient times and the interface  
198 conditions were dependent on the studied strategies as discussed in the next section. Their values  
199 are summarized in Table 1.

200 The effluent from  $^2\text{D}$  was split using a zero dead volume tee-piece (split 1:2; MS:UV). UV  
201 chromatograms were recorded at 210 nm with an acquisition rate of 80 Hz in  $^2\text{D}$ . QTOF-HRMS data  
202 were acquired in positive ion mode from 100 to 3200 m/z with an acquisition rate of 20 spectra/s.  
203 The drying gas temperature and flow rate were 300°C and 11 L/min, respectively. The nebulizer gas  
204 pressure was 40 psi. The sheath gas temperature and flow rate were 350 °C and 11 L/min,

205 respectively. The capillary, the nozzle, the fragmentor, the skimmer, and the Oct 1 RV voltages were  
 206 3500, 300, 150, 20, and 750 V, respectively.

207

## 208 2.5. Calculations

209

210 The effective peak capacities,  $n_{2D,eff}$ , were calculated from the following relationship:

$$211 \quad n_{2D,eff} = \alpha \times \gamma \times \left(1 + \frac{1\Delta t}{1w_{4\sigma}}\right) \times \left(1 + \frac{2\Delta t}{2w_{4\sigma}}\right) \quad (1)$$

212  $\Delta t$  is the whole range of elution times,  $w_{4\sigma}$ , the average peak width at  $4\sigma$  (i.e. 13.4% of peak height).

213  $\alpha$  corrects for undersampling in  $1D$  [27] and  $\gamma$  corrects for partial retention space coverage [28]. In all

214 present 2D-separations, their values were found to be 0.67 for  $\alpha$  and 1 for  $\gamma$  (100% coverage),

215 respectively.

216 The composition of acetonitrile at elution was calculated according to

$$217 \quad C_{elution} = C_{initial} + \frac{(C_{final} - C_{initial})}{t_G} (t_r - t_D - t_0) \text{ in RPLC}$$

218 Or

$$219 \quad C_{elution} = 100 - \left[ C_{initial} + \frac{(C_{final} - C_{initial})}{t_G} (t_r - t_D - t_0) \right] \text{ in HILIC} \quad (2)$$

220 Where  $C_{initial}$  and  $C_{final}$  are the initial and final compositions of acetonitrile in the mobile phase,  $t_r$  is

221 the retention time,  $t_D$  is the total dwell time, and  $t_0$  is the column dead time.

222 2D-data were processed with Matlab (V7.12.0635).

223 The following asymmetry factor,  $A_f$  was considered to assess the peak asymmetry:

$$224 \quad A_f = \frac{a+b}{2a} \quad (3)$$

225 With  $a$  and  $b$  the left and the right half peak width respectively, both measured at 5% of the peak  
 226 height.

227

228

## 229 3. Results and discussion

230

231 The objective of this study was to compare four strategies that are currently proposed to reduce

232 broad and distorted peaks and hence to improve the separation in the second dimension of on-line

233 HILIC x RPLC. We considered the peak shape, the peak width, and the peak capacity as the main

234 quality descriptors. The peak intensity and hence the extent to which the analytes were diluted was

235 also compared between the four strategies. Broad and distorted peaks mainly arise from a

236 difference in solvent strength between the organic-rich fraction coming from HILIC and the water-

rich mobile phase in RPLC. The four studied strategies included: (i) the Total Breakthrough strategy (TBS), which consists in injecting the entire fractions coming from <sup>1</sup>D so that a situation of Total Breakthrough occurs in <sup>2</sup>D for all peaks [13], (ii) The flow splitting strategy (FSS), which consists in splitting the flow prior to the valve and hence in injecting small volumes of undiluted fractions, and (iii) the make-up flow strategy (MFS) and (iv) the active solvent modulation strategy (ASMS). Both latter strategies result in injecting large volumes of fractions previously diluted with a weak solvent (usually water). This is carried out with a make-up pump in the first case and the ASM-valve (marketed by Agilent) in the second case. It should be noted that dilution after the switching valve was also recently reported under the name “at-column dilution” [21,22]. In this study, we considered the critical case in which the same column internal diameters (i.e. here 2.1 mm) are used in both dimensions. However, it should be noted that FSS with a split ratio of 1/10 should give similar results as those obtained with a ratio of 3 between the internal diameters (e.g. 1 mm in <sup>1</sup>D and 3 mm in <sup>2</sup>D). The studied sample was a tryptic digest of six proteins. Some conditions were specific to the studied strategy, including the gradient time in <sup>2</sup>D and other specific interface conditions. The other conditions, optimized in a previous study [13], are given in the experimental section.

253

### 3.1. Preliminary considerations and operating conditions for the four strategies

255

In on-line LC x LC, the continuous transfer of fractions from <sup>1</sup>D to <sup>2</sup>D is achieved by a switching-valve equipped with two sample loops. The interfaces for the four studied strategies are schematically represented in Fig. 1. While a fraction is stored in the first loop, the fraction previously stored in the second loop is injected and analysed in <sup>2</sup>D. The sampling time (i.e. the storage time) represents the total analysis time in <sup>2</sup>D (<sup>2</sup>t). To essentially maintain the resolution obtained in <sup>1</sup>D while ensuring a sufficient peak capacity in <sup>2</sup>D, the ratio of the sampling time to the <sup>1</sup>D-peak standard deviation (<sup>1</sup>σ) must be at least 2 [29,30] and sometimes up to 6 in case of sub-hour separations [31]. The sampling time and hence the analysis time in <sup>2</sup>D must be short (typically <sup>2</sup>t < 0.5 min for sub-hour separations). It includes different times. Their repartition is schematically represented in Fig. 2 for the four different strategies.

With TBS, FSS, and MFS, the available gradient time in <sup>2</sup>D is related to these different times according to:

$${}^2t_G = {}^2t - ({}^2t_{loop} + {}^2t_{D,instrum} + {}^2t_{post} + {}^2t_{eq}) \quad (4)$$

<sup>2</sup>t<sub>loop</sub> is the time required for the <sup>2</sup>D-mobile phase to travel across the sample loop (<sup>2</sup>t<sub>loop</sub> = <sup>2</sup>V<sub>loop</sub> / <sup>2</sup>F, with <sup>2</sup>V<sub>loop</sub> the loop volume and <sup>2</sup>F, the flow-rate in <sup>2</sup>D). <sup>2</sup>t<sub>D,instrum</sub> is the

270

271 instrument dwell time without considering the sample loop ( ${}^2t_D = {}^2t_{loop} + {}^2t_{D,instrum}$ ).  ${}^2t_{post}$  is  
 272 the short time required for going back to the initial composition and  ${}^2t_{eq}$ , the column equilibration  
 273 time. Both  ${}^2t_{post}$  and  ${}^2t_{eq}$  can be expressed as multiple of the column dead time ( ${}^2t_0$ ), typically one  ${}^2t_0$   
 274 and two  ${}^2t_0$ , respectively [32].

275 Whereas  ${}^2t_{D,instrum}$ ,  ${}^2t_{post}$  and  ${}^2t_{eq}$  cannot be further modified once properly selected,  ${}^2t_{loop}$  will  
 276 depend on the loop volume and hence on the selected strategy. Thus, according to Eq.4, the  
 277 maximum gradient time that can be used will also depend on the selected strategy.

278 With FSS (Fig.1b), the flow-rate coming from  ${}^1D$  ( ${}^1F$ ), is split with a desired split ratio ( $z_{split} < 1$ ) using a  
 279 tee-piece placed between the  ${}^1D$ -column outlet and the valve inlet.

280 With MFS (Fig.1c), the dilution of the fractions is achieved by continuously mixing the mobile phase  
 281 coming from  ${}^1D$  with a weak solvent delivered by an additional pump. Its flow rate is given by:

$$282 \quad F_{pump} = (z_{dilution} - 1) \times {}^1F \quad (5)$$

283 Where  ${}^1F$  is the flow-rate in  ${}^1D$  and  $z_{dilution}$  is the desired dilution ratio ( $> 1$ ).

284 With ASMS (Fig.1d), dilution of  ${}^1D$  fractions is achieved with a specific four-position switching-valve  
 285 equipped with restriction capillaries [19]. Different capillaries are available for adjusting the split  
 286 ratio and thus the dilution. The interface and the way it operates are schematically represented in  
 287 Figs. S2 and S3 of Supplementary Information. Compared to the standard valve (Fig. S1), the ASM  
 288 valve displays two additional positions (A and C) and two additional ports (5' and 6'), all involved in  
 289 the dilution process. The basic principle of ASMS is to make use of the initial  ${}^2D$ -mobile phase for  
 290 diluting the fraction volume. It is achieved by using a bypass capillary between the ports 5' and 6'  
 291 (Figs. S2 and S3b). In position A, the flow coming from the  ${}^2D$  pump is divided into two distinct paths.  
 292 In one path (port 5 to 7), the mobile phase goes through the loop to empty its content, whereas in  
 293 the other path (port 5 to 4), it goes through the bypass capillary. Depending on the selected bypass  
 294 capillary, the content of the sample loop is more or less diluted by the  ${}^2D$  mobile phase when the  
 295 two paths meet in port 6. After the dilution step, the ASM valve is switched back to the regular flow  
 296 path (position B) for analysis. The desired dilution factor ( $z_{dilution}$ ), is determined by the capillary  
 297 dimensions.

298 Regardless of the strategy, the injection volume in  ${}^2D$  ( ${}^2V_{injection}$ ) and the composition of the injection  
 299 solvent ( $C_{injection}$ ) can be expressed as:

300

$$301 \quad {}^2V_{injection} = {}^1F \times {}^2t \times z_{dilution} \times {}^1z_{split} \quad (6)$$

302 And

$$303 \quad C_{injection} = \frac{{}^1C_e + C_{dilution} \times (z_{dilution} - 1)}{z_{dilution}} \quad (7)$$

304 With  $C_{dilution}$ , the composition of strong solvent in the diluting solvent.

305  $z_{dilution} > 1$  with MFS or ASMS; =1 otherwise

306  $z_{split} < 1$  with FSS; =1 otherwise

307 It was often shown that the peak injection compression factor,  $C_F$ , which expresses how much the  
308 injection plug is reduced ( $C_F > 1$ ) or broadened ( $C_F < 1$ ) into the column, is directly related to the ratio  
309 of the retention factor in the injection solvent ( $k_s$ ) to the retention factor in the mobile phase at  
310 elution ( $k_e$ ) [17,33,34]:

$$311 \quad C_F = \frac{k_s}{k_e} \quad (8)$$

312 For this reason, the difference,  $\Delta C$ , between the composition of the injection solvent and the  
313 composition at peak elution, can be considered as a measure of the solvent strength mismatch:

$$314 \quad \Delta C = C_{injection} - C_e \quad (9)$$

315 Solvent strength mismatch is favourable when  $\Delta C < 1$ . It is all the more critical as  $\Delta C$  is much higher  
316 than 1.

317 With ASM, the duration of the dilution step and hence the required dilution volume must be  
318 specified. This latter must be at least equal to  ${}^2V_{injection}$ . However, a larger volume, expressed as a  
319 multiple,  $\lambda_{injection}$ , of  ${}^2V_{injection}$  (with  $\lambda_{injection} > 1$ ) is recommended to ensure the complete  
320 dilution of the fraction stored in the loop. It should be noted that the settable parameter required by  
321 the software is the number of loop volumes ( $\lambda_{loop}$ ) in place of the number of injection  
322 volumes ( $\lambda_{injection}$ ). It can be derived from the desired  $\lambda_{injection}$  by:

$$323 \quad \lambda_{loop} = \lambda_{injection} \times \frac{{}^1F \times {}^2t}{V_{loop}}$$

324 (10)

325 A value of 3 is recommended for  $\lambda_{loop}$  by Agilent. However, this value is most often too high  
326 considering the very short cycle times needed in sub-hour on-line LC x LC. To dilute the injection plug  
327 with the initial mobile phase, an initial isocratic hold has to be included in the pump program so that  
328 the gradient starts after the dilution step. Its duration,  ${}^2t_{iso}$ , is recommended to be the same as that  
329 of the dilution step and hence given by:

$$330 \quad {}^2t_{iso} = \frac{\lambda_{injection} \times {}^2V_{injection}}{{}^2F} \quad (11)$$

331 The analysis time in  ${}^2D$  using ASMS includes this initial hold and consequently, the available gradient  
332 time is decreased compared to Eq.4 according to:

$$333 \quad {}^2t_G = {}^2t - ({}^2t_{loop} + {}^2t_{D,instrum} + {}^2t_{iso} + {}^2t_{post} + {}^2t_{eq}) \quad (12)$$

334 As a rule of thumb, the volume occupied by the fraction in the loop,  $V_{fraction}$ , should not exceed  
335 two-thirds of the loop volume ( $V_{loop} \geq 1.5 \times V_{fraction}$ ) to take into account the molecular  
336 dispersion due to the parabolic flow. With ASMS, because the dilution is achieved after the sample  
337 loop,  $V_{fraction}$  is the same as with TBS (*i.e.*  ${}^1F \times {}^2t$ ) whereas with FSS and MFS, it corresponds

338 to the injection volume (Eq. 6). Whereas small loop volumes can be used with FSS ( $z_{\text{split}} < 1$ ) or even  
339 with TBS or ASMS, larger ones are required with MFS ( $z_{\text{dilution}} > 1$ ). Accordingly, the available time for  
340 the gradient is shorter (Fig.2). Of greater practical consequence is the fact that the peak capacity is  
341 expected to be lower since the peak capacity decreases with the gradient time.

342

343 The interface conditions for the four different strategies and the remaining gradient times are listed  
344 in Table 1. For a fair comparison, the chromatographic conditions were basically the same and quite  
345 close to those previously applied to the on-line HILIC x RPLC analysis of a tryptic digest [13]. The  
346 gradient time in <sup>1</sup>D (assumed to be the analysis time) was 30 min. The analysis time in <sup>2</sup>D (i.e. the  
347 sampling time) was 0.39 min. The flow-rate in <sup>2</sup>D (i.e. 2 mL/min) was fixed in such a way that the  
348 maximum allowable pressure (i.e. 1000 bar) could be reached. The sample loop volumes were  
349 selected among commercially available loops so that the injection volume did not exceed two-thirds  
350 of the loop volume. As shown in Fig. 2, some times during the run in <sup>2</sup>D were maintained identical  
351 for the four studied strategies. Those include  ${}^2t_{D,\text{instrum}}$ ,  ${}^2t_{\text{post}}$ , and  ${}^2t_{\text{eq}}$  equal to 0.022, 0.030 and 0.058  
352 min, respectively. Accordingly, interface conditions being different, the gradient times in <sup>2</sup>D (Table 1)  
353 were also different depending on the strategy (see Eqs. 4 and 10).

354

355 With TBS (Figs. 1a and 2), no additional device is required, making this strategy very easy to operate.  
356 The whole fraction coming from <sup>1</sup>D was injected in <sup>2</sup>D. That resulted in relatively large volumes of  
357 strong solvent injected in <sup>2</sup>D. For the separation of peptides, the percentage of ACN in the HILIC  
358 fractions was between 98% and 48% depending on the solute retention in HILIC. A conventional two-  
359 position/4-port duo-valve was used in the backflush mode (Fig. S1). Considering the flow rate in <sup>1</sup>D  
360 (i.e. 50  $\mu\text{L}/\text{min}$ ) and the sampling time of 0.39 min, the volume of each transferred fraction and  
361 hence the volume injected in <sup>2</sup>D, was exactly 19.5  $\mu\text{L}$ . That represented about 27%  ${}^2V_0$  ( ${}^2V_0$  being the  
362 <sup>2</sup>D-column dead volume). Considering commercially available loop sizes and with respect to a filling  
363 percentage of no more than 66%, the selected sample loop volume was 40  $\mu\text{L}$ . Accordingly,  ${}^2t_{\text{loop}}$  was  
364 0.02 min, resulting in a gradient time of 0.26 min (Eq. 4).

365

366 With FSS (Figs. 1b and 2), restriction capillaries were mounted to provide a split 1:9 ( $z_{\text{split}} = 0.1$ ), thus  
367 allowing sending nine-tenths of the flow to the waste while one-tenth to the sample loop. As said  
368 above, a split ratio of 1/10 with similar inner diameters (I.D) in both dimensions (e.g.. 2.1 mm)  
369 mimics a situation in which the column I.D ratio would be close to 3 (e.g. 1 mm in <sup>1</sup>D and 3 mm in  
370 <sup>2</sup>D). Under these conditions, the injected volume in the second dimension was exactly 1.95  $\mu\text{L}$ . That  
371 represents about 2.7%  $V_0$ . By reducing the loop volume down to the lowest available standardized

372 loop volume (i.e. 20  $\mu\text{L}$ ), the gain in time was rather small (of the order of 0.01 min) but allowed for  
373 a very small increase in the gradient time (0.27 min).

374

375 With both MFS and ASMS, a dilution ratio of 5 (maximum dilution ratio with ASMS) was selected.  
376 This one was recommended in case of strong solvent strength mismatch [19]. A lower dilution ratio  
377 would reduce the transfer volume (Eq. 6) but also increase the injection solvent strength (Eq. 7).

378 With MFS (Figs. 1c and 2) and a dilution ratio of five,  $F_{\text{pump}}$  was 200  $\mu\text{L}/\text{min}$  (Eq.2). The diluting  
379 solvent composition was the same as for the starting composition of the <sup>2</sup>D mobile phase (i.e. 1%  
380 ACN + 0.1% FA and 99% water + 0.1% FA). In these conditions, the percentage of ACN in the injection  
381 solvent was decreased from 98% to 20.4% in <sup>1</sup>D initial conditions and from 52% to 11.2% in <sup>1</sup>D final  
382 conditions (Eq. 7). The fraction volume, entering the valve was multiplied by 5 (i.e. 97.5  $\mu\text{L}$ ) thus  
383 requiring a larger loop volume than previously (i.e. 180  $\mu\text{L}$ ). As a consequence,  ${}^2t_{\text{loop}}$  and thus  ${}^2t_{\text{G}}$   
384 became 0.09 min and 0.19 min, respectively. The available gradient time with this approach was  
385 about 27% smaller than with the two preceding ones (0.19 min vs. 0.26 or 0.27 min).

386

387 With ASMS (Figs. 1D and 2), dilution is carried out without additional pump. A specific ASM-valve  
388 allows diluting the collected fractions inside the valve itself. As a result, the fraction volume entering  
389 the valve was the same as with TBS (i.e. 19.5  $\mu\text{L}$ ), needing the same loop volume of 40  $\mu\text{L}$ .  
390 Considering the sample loop volume, twice as large as the fraction volume, only one sample loop  
391 volume ( $\lambda_{\text{loop}} = 1$  and  $\lambda_{\text{injection}}$  close to 2) was used to flush the loop. As a result and according to Eq.  
392 11, a dilution step and hence an isocratic hold ( ${}^2t_{\text{iso}}$ ) of 0.1 min was required for complete sample  
393 dilution which, according to Eq. 12, reduced the available gradient time by about 16% compared to  
394 MFS (0.16 min vs. 0.19 min).

395

### 396 3.2. On-line HILIC x RPLC with TBS or FSS

397

398 The main difference between FSS and TBS is the use of restriction capillaries with FSS which divides  
399 the flow before entering the valve. This results in lower injection volumes (here ten-fold lower than  
400 with TBS). With TBS, as discussed above, the injection volumes in <sup>2</sup>D are large enough to attain a  
401 situation of Total Breakthrough for all peptides. As previously defined [13], Total Breakthrough exists  
402 when there are only two distinct peaks for a given solute, the first one unretained (breakthrough)  
403 and the second one retained and quite symmetrical. It was found for peptides that Total  
404 Breakthrough occurs when the injection volume is higher than a critical one. For smaller volumes, a

405 transition step was pointed out, in which breakthrough occurs while the retained peak is distorted  
406 and sometimes split.

407 Fig. 3 shows the 2D-contour plots obtained for the separations of the tryptic digest with TBS (Figs.  
408 3a) and FSS (Figs. 3b), with a view centred on the useful separation space. The entire 2D-contour  
409 plots are shown in Fig. S4. The 3D-plots are given in Fig. S5 to compare the peak intensities of the  
410 two separations. With TBS, an intense and large band appears between 2 and 3 seconds. It  
411 corresponds to the expected <sup>2</sup>D-column dead time (about 2.2 s) and is therefore composed of peaks  
412 of breakthrough as also confirmed by HRMS. Those are omnipresent in <sup>2</sup>D during the entire <sup>1</sup>D  
413 separation. As can be observed, they do not enter the separation space delimited by dotted lines.  
414 With FSS, despite a much lower injection volume (1.95  $\mu$ L vs. 19.5  $\mu$ L), some peaks of breakthrough  
415 are still present, although less intense than with TBS (Fig. 3b vs. Fig.3a). This is not surprising since  
416 breakthrough has been observed for peptides in on-line HILIC x RPLC with injection volumes as low  
417 as 2%  $V_0$  [8]. Breakthrough could have been mitigated provided that lower volumes had been  
418 injected in <sup>2</sup>D. In our case, this could have been done by means of larger split ratios between the two  
419 dimensions (e.g. 1/26 for  $V_i = 1\% V_0$ ). Nevertheless, we do not believe that breakthrough could have  
420 been eliminated given that its occurrence was reported with injected volumes as low as 0.5%  $V_0$   
421 under similar chromatographic conditions [13]. Furthermore, such a decrease in injection volume  
422 would have significantly impacted the method sensitivity, as will be underlined in the subsequent  
423 section.

424 As shown by dotted lines in Fig.3, the entire separation space is occupied by peaks in HILIC x RPLC  
425 (i.e.  $\gamma = 1$  in Eq.1). Key values for the effective peak capacity calculation (Eq. 1) are listed in Table 2.  
426 The average peak widths in <sup>1</sup>D and <sup>2</sup>D (UV detection) were assessed from about fifty single  
427 symmetrical peaks. The conditions in <sup>1</sup>D being the same with the four strategies, <sup>1</sup> $\Delta t$  and <sup>1</sup> $w_{4\sigma}$  values  
428 are the same. <sup>2</sup> $\Delta t$  is slightly larger with FSS but the main difference comes from average <sup>2</sup> $w_{4\sigma}$  values  
429 (0.39 s with TBS vs. 0.46 s with FSS), resulting in a higher peak capacity (i.e. 1100 with TBS vs. 970  
430 with FSS). As discussed before, TBS ensures a situation of Total Breakthrough due to an injection  
431 volume well above the critical one for all peptides. With FSS, the injection volume is most time too  
432 low for Total Breakthrough but not low enough to avoid broadening, distortion or breakthrough, as  
433 will be further discussed. In addition to the effect of injection solvent strength, low split ratios (here  
434  $z_{split} = 0.1$ ) can also significantly broaden the peaks [35]. It is important to note that peak widths  
435 could only be measured on symmetrical peaks which makes the peak capacity of 970 very optimistic.  
436 3D-chromatograms bring attention to the significant difference in peak intensity between TBS (Fig.  
437 S5a) and FSS (Fig.S5b). This difference can also be assessed with the overlaid <sup>2</sup>D-chromatograms  
438 shown in Fig. S6. With a view to even better assess the difference in peak intensity between the

439 studied strategies, 39 different single peaks, identified by HRMS, were selected. Those peaks had to  
440 be well distributed among the whole retention space with a signal-to-noise ratio higher than five (UV  
441 detection) for accurate measurements. Their peak height ratios between TBS and FSS are listed in  
442 Table 3. The largest peak height ratios concerned the most retained peaks in <sup>2</sup>D. Their intensities  
443 were less affected since the intensity of the peak of breakthrough decreased as the peptide  
444 retention increased as earlier discussed [13]. On average, the peak intensity was found to be about  
445 8-fold higher with TBS, ranging from 3- to 22-fold. As seen in Table 2, about 99% of the expected  
446 peptides from the trypsin digestion (i.e. 237/238, including known post-translational modifications)  
447 were identified with HRMS detection for TBS. In comparison, only 86% (i.e. 205/238) could be  
448 unambiguously identified for FSS due to low detection sensitivity. These results underline the high  
449 dilution caused by FSS conditions.

450 Finally, considering both peak capacity (Table 2) and peak intensity (Table 3), TBS was proved to be a  
451 much better choice than FSS to reduce undesirable effects of strong injection solvents in the <sup>2</sup>D-  
452 RPLC.

453

### 454 3.3. On-line HILIC x RPLC with MFS or ASMS

455

456 Both strategies consist in diluting the injection plug with a weak solvent (here 1% ACN in water with  
457 0.1% FA). The eluent strength of the <sup>1</sup>D-effluent is therefore decreased before entering the <sup>2</sup>D-  
458 column to promote column focusing. On-line dilution was achieved before the switching valve (MFS)  
459 or inside the switching valve (ASMS). The contour plots and the 3D-chromatograms for both MFS  
460 and ASMS are shown in Fig. 3 and Fig. S5, respectively. The similarity between the two separations is  
461 noteworthy. As a consequence of the large isocratic hold before the gradient enters the column, a  
462 large empty space with MFS (Fig. 3c) and even larger with ASMS (Fig. 3d) is clearly observed. Since  
463 the sampling time was identical for all strategies, the available gradient time (Fig. 2) and hence the  
464 separation space (i.e. <sup>2</sup>Δt in Table 2) was inevitably much smaller compared to TBS or FSS (27% and  
465 40% smaller with MFS and ASMS, respectively). As could be expected, a smaller average peak width  
466 was obtained with both MFS and ASMS compared to FSS (Table 2). The average peak width was yet  
467 close to that with TBS. Due to the shorter <sup>2</sup>Δt with both dilution approaches, peak capacities were  
468 much smaller with MFS (770) and ASMS (680) than with TBS (1100) or even FSS (970). Furthermore,  
469 despite on-line dilution, intense peaks of breakthrough are still observed with MFS as well as with  
470 ASMS (Fig. 3), especially for moderately retained compounds in <sup>1</sup>D.

471 As seen in Fig. S5 and confirmed by Table 3, the peak heights of the retained peaks are similar  
472 between MFS and ASMS. On average, they were about five times higher than with TBS. The presence

473 of breakthrough did not seem to impair much the peak intensity. As seen in Table 2, the percentage  
474 of expected peptides identified with both strategies was the same as for TBS.

475 In the next section, the comparison of the peak shapes from HRMS detection will complete the  
476 evaluation of the four strategies.

477

#### 478 3.4. Comparison of peak shapes in on-line HILIC x RPLC with the four studied strategies

479

480 To provide an objective comparison of the peak shapes depending on the studied strategies,  
481 extracted ion chromatograms (EICs) of five relevant peptides are shown in Figs. 4 to 8. Each  
482 separation displays the most intense fraction among the two or three <sup>1</sup>D-peak fractions. The figures  
483 are ranged from the most retained peptide in <sup>2</sup>D (Fig. 4) to the least retained one (Fig. 8). The  
484 location of each peak is indicated on the 2D-maps in Fig. S4. Useful information, listed in Table 4,  
485 includes *m/z* values, retention times in both dimensions, compositions at elution in both dimensions  
486 (Eq. 2), compositions of the injection solvent in <sup>2</sup>D (Eq. 7), measured effective peak capacities (Eq. 1),  
487 observed type of separation (Total Breakthrough, single symmetrical peak, peak distortion, split  
488 peak, transition step accompanied by both peak distortion and breakthrough) and peak asymmetry  
489 factors (Eq. 3). Note that the effective peak capacities, as well as the asymmetry factors, could not  
490 be measured when the peak distortion was significant or when the peak intensity was too low. It  
491 should be pointed out that the effective peak capacities were calculated from MS-peak widths in  
492 Table 4 but from UV-peak widths in Table 2. The resulting lower values are due to significant  
493 additional solute dispersion between the UV-instrument and the Q-TOF-MS connected in parallel  
494 with a tee-piece.

495 Finally as previously said,  $\Delta C$  (Eq. 9) can be considered as a measure of the solvent strength  
496 mismatch and was therefore also reported in Table 4 as additional relevant characteristic.

497

498 The peptide in Fig. 4 is strongly retained in both dimensions. As a result, the injection solvent  
499 strength is moderate (57% and 54%ACN with TBS and FSS respectively) and more importantly,  $\Delta C$  is  
500 low with both TBS and FSS (i.e. 25%) and negative with both MFS and ASMS (i.e. -20%). As expected,  
501 a small peak of breakthrough appears with TBS. In such conditions, the retained peak is kept rather  
502 symmetrical with all strategies (i.e.  $1 \leq A_s \leq 1.6$ , except for ASMS). However, for the reasons already  
503 given above, the effective peak capacities are much lower with MFS and ASMS.

504 In Figs. 5 to 7, the peptides are poorly retained in <sup>1</sup>D (<sup>1</sup>*C*<sub>elution</sub> from 86% to 71%ACN) while moderately  
505 retained in <sup>2</sup>D (<sup>2</sup>*C*<sub>elution</sub> from 29% to 15% ACN), which results in high  $\Delta C$  values with TBS and FSS  
506 (about 60% ACN). With FSS, despite a very small injection volume, the peaks are split in Figs. 5b and

507 6b while Total Breakthrough similar to what is always observed with TBS can be observed in Fig. 7b.  
508 Regarding MFS and ASMS, the  $\Delta C$  values remain negative for the peptide in Fig. 5 (i.e. close to -10%),  
509 thus allowing a fairly symmetrical retained peak. However,  $\Delta C$  values seem to be too high for the  
510 peptides in Figs. 6 and 7, taking also into account the very large injection volume resulting from  
511 these strategies (i.e. 97.5 $\mu$ L). Peak fronting can be observed with MFS in Fig. 6c and a peak of  
512 breakthrough appears with ASMS in Fig. 6d, suggesting a transition step before a further situation of  
513 Total Breakthrough. The earlier emergence of breakthrough in the case of ASMS can be readily  
514 explained by the slight difference in  $\Delta C$  between the two strategies. In Fig. 7, the peaks are  
515 distorted with both MFS (Fig. 7c) and ASMS (Fig. 7d). In addition to the very bad peak shapes, a peak  
516 of breakthrough is present in both cases. This suggests that on-line dilution is not sufficient to  
517 circumvent the deleterious impact of solvent strength mismatch and thus to ensure symmetrical  
518 peaks. This bad separation can be related to the  $\Delta C$  values (here close to 0%), higher than for the  
519 peptide in Fig. 6 and much higher than for the peptide in Fig. 5.

520 Three approaches could be considered to reduce the transferred volume while maintaining the same  
521 dilution ratio (same  $\Delta C$ ): (i) splitting the flow-rate prior to the valve, (ii) sending part of the fraction  
522 to the waste by using loop volumes smaller than the fraction volume or (iii) using trapping columns.  
523 The first approach involves the combination of two strategies (FSS and on-line dilution). The second  
524 one could not strictly refer to as comprehensive 2D-LC and furthermore cannot be considered for  
525 quantitative analysis since the percentage of component sent in the second dimension may vary  
526 from run-to-run. Furthermore, these two approaches should result in a reduction of the peak heights  
527 (lower sensitivity). Regarding the use of trapping columns in combination with on-line dilution (MFS  
528 only), its benefit in terms of transferred volume reduction has never been clearly proved as above  
529 highlighted.

530 The last proposed example (Fig. 8) is interesting. In this case, the peptide is strongly retained in <sup>1</sup>D  
531 like the peptide in Fig. 6 (<sup>1</sup>C<sub>elution</sub> close to 60% ACN) but poorly retained in <sup>2</sup>D (<sup>2</sup>C<sub>elution</sub> close to 6%  
532 ACN). With both TBS and FSS (Figs. 8a and 8b), the situation of total breakthrough is attained. With  
533 MFS and ASMS (Figs. 8c and 8d), a transition step close to a situation of Total Breakthrough but with  
534 a low fronting between the peak of breakthrough and the retained peak can be observed. Once  
535 again, these results can be correlated to the high  $\Delta C$  values (here positive values close to 7% ACN). It  
536 is interesting to point out that the breakthrough peak is much larger with MFS (Fig. 8c) and ASMS  
537 (Fig.8d) than with TBS (Fig. 8a). It is the thinnest with FSS (8b). That is not surprising considering that  
538 the width of the non-retained breakthrough peak is expected to vary linearly with the injected  
539 volume.

540

541 Apart from obvious consequences on separation and sensitivity, the occurrence of breakthrough in  
542 each of these strategies raises the question of quantitative analysis. In our previous study [13], we  
543 observed a linear variation of the retained peak area with the amount of peptide injected, as soon as  
544 the situation of Total Breakthrough was attained. However, the variation was no more linear when  
545 the peak was eluted under the conditions of transition step (i.e. after the emergence of  
546 breakthrough but before Total Breakthrough). This suggests that quantitative analysis should be  
547 quite reliable with TBS while problematic with the three other strategies (transition step with FSS in  
548 Figs. 6b, with MFS in Fig. 7c or with ASMS in Fig. 7d).

549  
550 In summary, the following conclusions can be drawn from the separations shown in Figs. 4 to 8: (i)  
551 TBS was the only strategy ensuring fairly symmetrical peaks ( $1 \leq A_s \leq 1.6$ ) -for all peptides in on-line  
552 HILIC x RPLC, (ii) the success of the three other strategies (FSS, MFS, and ASMS), for a given peptide,  
553 strongly depended on  $\Delta C$  values which had to be low enough to avoid injection issues, (iii)  
554 considering that it was not possible to ensure sufficiently low  $\Delta C$  values for all peptides given the  
555 broad range of elution in both dimensions, the peak capacity and hence the quality of the separation  
556 was inevitably more or less affected with MFS and ASMS, and (iv) MFS and ASMS yielded quite  
557 similar results with the same dilution ratio.

558  
559 In this study, TBS was used for the separation of peptides. We are currently studying the occurrence  
560 of Total Breakthrough over a wider range of solutes (acidic and basic, multi-charged or not) and a  
561 wider range of chromatographic conditions (different stationary phases, different mobile phases,  
562 pHs, temperatures, gradient conditions). Our obtained results allow asserting that Total  
563 Breakthrough can also be attained with small monocharged molecules in RPLC. An example is given  
564 in figure S7 for propranolol. We hope to be able soon to publish a complete overview of the  
565 circumstances leading to the phenomenon of Total Breakthrough.

566

#### 567 **4. Concluding remarks**

568

569 In this study, we compared four strategies designed to reduce undesirable effects of strong injection  
570 solvents on peak shapes in the second dimension of on-line HILIC x RPLC for the separation of  
571 peptides: (i) the Total Breakthrough strategy (TBS) with injection of large volumes of raw fractions,  
572 (ii) the flow splitting strategy (FSS) with injection of low volumes of raw fractions, and two on-line  
573 dilution strategies with injection of very large volumes of diluted fractions, either (iii) with a make-up  
574 flow (MFS) or (iv) with an ASM-valve (ASMS). The quality of the separation was assessed on the basis

575 of peak shapes, peak capacity, and peak intensity. The comparison was made in the context of a  
576 separation of a complex peptide sample performed in 30 min by considering the most critical case  
577 where similar column inner diameters are used in both dimensions (i.e. 2.1 mm).

578 The best results in term of peak shapes and peak capacity were obtained with TBS. A feature of this  
579 strategy is that it deliberately copes with breakthrough, unlike the three other ones where  
580 breakthrough is highly critical. No additional device is required with TBS, making this strategy very  
581 easy to operate. A peak capacity of 1100 could be achieved within just half an hour. Due to both  
582 peak broadening and a reduction of the separation space in <sup>2</sup>D, the obtained peak capacity was more  
583 than 40% lower with the on-line dilution strategies. Unlike TBS, it was shown that neither a split ratio  
584 of 1/10 (FSS) nor a dilution ratio of 5 (MFS and ASMS) were sufficient to provide symmetrical peaks  
585 across the entire 2D-separation space and hence to avoid excessive band broadening, fronting, split  
586 peaks, and breakthrough.

587 The difference in composition between the injection solvent and the mobile phase at peak elution  
588 ( $\Delta C$ ) in combination with the injection volume was found to be related to the extent to which peaks  
589 are distorted and also to the occurrence of breakthrough. Above a critical  $\Delta C$  value depending on  
590 the injection volume, a situation of Total Breakthrough takes place. Due to low  $\Delta C$  values, this  
591 situation was rarely attained with MFS or with ASMS.

592 On average the peak intensity was five times higher with the on-line dilution strategies than with  
593 TBS. However, TBS led to much better results than FSS, with an eight-fold increase in peak intensity.  
594 This highlights the poor sensitivity involved by FSS while this strategy is still the most reported one in  
595 on-line HILIC x RPLC.

596 ASMS and MFS gave very similar results. Both techniques need an additional device, either an ASM  
597 valve or an isocratic pump (MFS). This latter solution benefits from easy implementation.  
598 Furthermore, the present study shows that the current limitation for the dilution ratio (not higher  
599 than 5) in the case of the ASM valve can be a critical issue for the quality of the separation in on-line  
600 HILIC x RPLC.

601 Finally, there are many ways to compare the different strategies for given <sup>1</sup>D conditions. The  
602 quality descriptors are multiple (peak height, peak width, peak capacity, peak asymmetry...).  
603 Depending on the objectives, one of the descriptors may prevail over another. However  
604 peak heights, peak widths and hence peak capacity cannot be assessed if the peaks are  
605 distorted. The first objective of the analyst should therefore be to obtain only quasi-  
606 symmetrical peaks. The main conclusion of this study on HILIC x RPLC is that this objective  
607 can only be achieved with TBS.

608

609 **Acknowledgements**

610

611 The authors gratefully acknowledge Agilent technologies for the loan of the 2D-LC instrument and  
612 the Active Solvent Modulation 2D-LC valve.

613

614 **References**

615

- 616 [1] Y.Z. Baghdady, K.A. Schug, Online Comprehensive High pH Reversed Phase × Low  
617 pH Reversed Phase Approach for Two-Dimensional Separations of Intact Proteins in  
618 Top-Down Proteomics, *Anal. Chem.* 91 (2019) 11085–11091.  
619 <https://doi.org/10.1021/acs.analchem.9b01665>.
- 620 [2] M. Muller, A.G.J. Tredoux, A. de Villiers, Predictive kinetic optimisation of hydrophilic  
621 interaction chromatography × reversed phase liquid chromatography separations:  
622 Experimental verification and application to phenolic analysis, *Journal of*  
623 *Chromatography A.* 1571 (2018) 107–120.  
624 <https://doi.org/10.1016/j.chroma.2018.08.004>.
- 625 [3] M. Muller, A.G.J. Tredoux, A. de Villiers, Application of Kinetically Optimised Online  
626 HILIC × RP-LC Methods Hyphenated to High Resolution MS for the Analysis of  
627 Natural Phenolics, *Chromatographia.* 82 (2019) 181–196.  
628 <https://doi.org/10.1007/s10337-018-3662-6>.
- 629 [4] B.W.J. Pirok, N. Abdulhussain, T. Brooijmans, T. Nabuurs, J. de Bont, M.A.J.  
630 Schellekens, R.A.H. Peters, P.J. Schoenmakers, Analysis of charged acrylic particles by  
631 on-line comprehensive two-dimensional liquid chromatography and automated data-  
632 processing, *Analytica Chimica Acta.* 1054 (2019) 184–192.  
633 <https://doi.org/10.1016/j.aca.2018.12.059>.
- 634 [5] M. Iguiniz, E. Corbel, N. Roques, S. Heinisch, Quantitative aspects in on-line  
635 comprehensive two-dimensional liquid chromatography for pharmaceutical  
636 applications, *Talanta.* 195 (2019) 272–280.  
637 <https://doi.org/10.1016/j.talanta.2018.11.030>.
- 638 [6] M. Sarrut, A. Corgier, S. Fekete, D. Guillarme, D. Lascoux, M.-C. Janin-Bussat, A.  
639 Beck, S. Heinisch, Analysis of antibody-drug conjugates by comprehensive on-line two-  
640 dimensional hydrophobic interaction chromatography × reversed phase liquid  
641 chromatography hyphenated to high resolution mass spectrometry. I – Optimization of  
642 separation conditions, *Journal of Chromatography B.* 1032 (2016) 103–111.  
643 <https://doi.org/10.1016/j.jchromb.2016.06.048>.
- 644 [7] A. Ehkirch, V. D’Atri, F. Rouviere, O. Hernandez-Alba, A. Goyon, O. Colas, M. Sarrut,  
645 A. Beck, D. Guillarme, S. Heinisch, S. Cianferani, An Online Four-Dimensional  
646 HIC×SEC-IM×MS Methodology for Proof-of-Concept Characterization of Antibody  
647 Drug Conjugates, *Anal. Chem.* 90 (2018) 1578–1586.  
648 <https://doi.org/10.1021/acs.analchem.7b02110>.
- 649 [8] G. Vanhoenacker, I. Vandenheede, F. David, P. Sandra, K. Sandra, Comprehensive two-  
650 dimensional liquid chromatography of therapeutic monoclonal antibody digests, *Anal*  
651 *Bioanal Chem.* 407 (2015) 355–366. <https://doi.org/10.1007/s00216-014-8299-1>.
- 652 [9] L. Montero, V. Sáez, D. von Baer, A. Cifuentes, M. Herrero, Profiling of *Vitis vinifera*  
653 *L. canes* (poly)phenolic compounds using comprehensive two-dimensional liquid  
654 chromatography, *Journal of Chromatography A.* 1536 (2018) 205–215.  
655 <https://doi.org/10.1016/j.chroma.2017.06.013>.

- 656 [10] H. Zhang, J.-M. Jiang, D. Zheng, M. Yuan, Z.-Y. Wang, H.-M. Zhang, C.-W. Zheng,  
657 L.-B. Xiao, H.-X. Xu, A multidimensional analytical approach based on time-decoupled  
658 online comprehensive two-dimensional liquid chromatography coupled with ion  
659 mobility quadrupole time-of-flight mass spectrometry for the analysis of ginsenosides  
660 from white and red ginsengs, *Journal of Pharmaceutical and Biomedical Analysis*. 163  
661 (2019) 24–33. <https://doi.org/10.1016/j.jpba.2018.09.036>.
- 662 [11] J.-L. Cao, S.-S. Wang, H. Hu, C.-W. He, J.-B. Wan, H.-X. Su, Y.-T. Wang, P. Li,  
663 Online comprehensive two-dimensional hydrophilic interaction  
664 chromatography×reversed-phase liquid chromatography coupled with hybrid linear ion  
665 trap Orbitrap mass spectrometry for the analysis of phenolic acids in *Salvia miltiorrhiza*,  
666 *Journal of Chromatography A*. 1536 (2018) 216–227.  
667 <https://doi.org/10.1016/j.chroma.2017.09.041>.
- 668 [12] A. Martín-Ortiz, A.I. Ruiz-Matute, M.L. Sanz, F.J. Moreno, M. Herrero, Separation of  
669 di- and trisaccharide mixtures by comprehensive two-dimensional liquid  
670 chromatography. Application to prebiotic oligosaccharides, *Analytica Chimica Acta*.  
671 1060 (2019) 125–132. <https://doi.org/10.1016/j.aca.2019.01.040>.
- 672 [13] S. Chapel, F. Rouvière, S. Heinisch, Pushing the limits of resolving power and analysis  
673 time in on-line comprehensive hydrophilic interaction x reversed phase liquid  
674 chromatography for the analysis of complex peptide samples, *Journal of*  
675 *Chromatography A*. (2019) 460753. <https://doi.org/10.1016/j.chroma.2019.460753>.
- 676 [14] S. Toro-Uribe, L. Montero, L. López-Giraldo, E. Ibáñez, M. Herrero, Characterization  
677 of secondary metabolites from green cocoa beans using focusing-modulated  
678 comprehensive two-dimensional liquid chromatography coupled to tandem mass  
679 spectrometry, *Analytica Chimica Acta*. 1036 (2018) 204–213.  
680 <https://doi.org/10.1016/j.aca.2018.06.068>.
- 681 [15] L. Montero, E. Ibáñez, M. Russo, L. Rastrelli, A. Cifuentes, M. Herrero, Focusing and  
682 non-focusing modulation strategies for the improvement of on-line two-dimensional  
683 hydrophilic interaction chromatography × reversed phase profiling of complex food  
684 samples, *Analytica Chimica Acta*. 985 (2017) 202–212.  
685 <https://doi.org/10.1016/j.aca.2017.07.013>.
- 686 [16] E. Sommella, O.H. Ismail, F. Pagano, G. Pepe, C. Ostacolo, G. Mazzocanti, M. Russo,  
687 E. Novellino, F. Gasparrini, P. Campiglia, Development of an improved online  
688 comprehensive hydrophilic interaction chromatography × reversed-phase ultra-high-  
689 pressure liquid chromatography platform for complex multiclass polyphenolic sample  
690 analysis, *J. Sep. Sci.* 40 (2017) 2188–2197. <https://doi.org/10.1002/jssc.201700134>.
- 691 [17] M. Sarrut, A. D’Attoma, S. Heinisch, Optimization of conditions in on-line  
692 comprehensive two-dimensional reversed phase liquid chromatography. Experimental  
693 comparison with one-dimensional reversed phase liquid chromatography for the  
694 separation of peptides, *Journal of Chromatography A*. 1421 (2015) 48–59.  
695 <https://doi.org/10.1016/j.chroma.2015.08.052>.
- 696 [18] P. Venter, M. Muller, J. Vestner, M.A. Stander, A.G.J. Tredoux, H. Pasch, A. de  
697 Villiers, Comprehensive Three-Dimensional LC × LC × Ion Mobility Spectrometry  
698 Separation Combined with High-Resolution MS for the Analysis of Complex Samples,  
699 *Anal. Chem.* 90 (2018) 11643–11650. <https://doi.org/10.1021/acs.analchem.8b03234>.
- 700 [19] D.R. Stoll, K. Shoykhet, P. Petersson, S. Buckenmaier, Active Solvent Modulation: A  
701 Valve-Based Approach To Improve Separation Compatibility in Two-Dimensional  
702 Liquid Chromatography, *Anal. Chem.* 89 (2017) 9260–9267.  
703 <https://doi.org/10.1021/acs.analchem.7b02046>.
- 704 [20] D.R. Stoll, D.C. Harmes, G.O. Staples, O.G. Potter, C.T. Dammann, D. Guillarme, A.  
705 Beck, Development of Comprehensive Online Two-Dimensional Liquid

- 706 Chromatography/Mass Spectrometry Using Hydrophilic Interaction and Reversed-Phase  
707 Separations for Rapid and Deep Profiling of Therapeutic Antibodies, *Anal. Chem.* 90  
708 (2018) 5923–5929. <https://doi.org/10.1021/acs.analchem.8b00776>.
- 709 [21] Y. Chen, J. Li, O.J. Schmitz, Development of an At-Column Dilution Modulator for  
710 Flexible and Precise Control of Dilution Factors to Overcome Mobile Phase  
711 Incompatibility in Comprehensive Two-Dimensional Liquid Chromatography, *Anal.*  
712 *Chem.* 91 (2019) 10251–10257. <https://doi.org/10.1021/acs.analchem.9b02391>.
- 713 [22] Y. Chen, L. Montero, J. Luo, J. Li, O.J. Schmitz, Application of the new at-column  
714 dilution (ACD) modulator for the two-dimensional RP×HILIC analysis of *Buddleja*  
715 *davidii*, *Anal Bioanal Chem.* 412 (2020) 1483–1495. [https://doi.org/10.1007/s00216-](https://doi.org/10.1007/s00216-020-02392-3)  
716 [020-02392-3](https://doi.org/10.1007/s00216-020-02392-3).
- 717 [23] D.R. Stoll, E.S. Talus, D.C. Harmes, K. Zhang, Evaluation of detection sensitivity in  
718 comprehensive two-dimensional liquid chromatography separations of an active  
719 pharmaceutical ingredient and its degradants, *Anal Bioanal Chem.* 407 (2015) 265–277.  
720 <https://doi.org/10.1007/s00216-014-8036-9>.
- 721 [24] B.W.J. Pirok, D.R. Stoll, P.J. Schoenmakers, Recent Developments in Two-  
722 Dimensional Liquid Chromatography: Fundamental Improvements for Practical  
723 Applications, *Analytical Chemistry.* 91 (2019) 240–263.  
724 <https://doi.org/10.1021/acs.analchem.8b04841>.
- 725 [25] A.F.G. Gargano, M. Duffin, P. Navarro, P.J. Schoenmakers, Reducing Dilution and  
726 Analysis Time in Online Comprehensive Two-Dimensional Liquid Chromatography by  
727 Active Modulation, *Anal. Chem.* 88 (2016) 1785–1793.  
728 <https://doi.org/10.1021/acs.analchem.5b04051>.
- 729 [26] E. Sommella, E. Salviati, S. Musella, V. Di Sarno, F. Gasparrini, P. Campiglia,  
730 Comparison of Online Comprehensive HILIC × RP and RP × RP with Trapping  
731 Modulation Coupled to Mass Spectrometry for Microalgae Peptidomics, *Separations.* 7  
732 (2020) 25. <https://doi.org/10.3390/separations7020025>.
- 733 [27] J.M. Davis, D.R. Stoll, P.W. Carr, Effect of First-Dimension Undersampling on  
734 Effective Peak Capacity in Comprehensive Two-Dimensional Separations, *Anal. Chem.*  
735 80 (2008) 461–473. <https://doi.org/10.1021/ac071504j>.
- 736 [28] A. D'Attoma, C. Grivel, S. Heinisch, On-line comprehensive two-dimensional  
737 separations of charged compounds using reversed-phase high performance liquid  
738 chromatography and hydrophilic interaction chromatography. Part I: Orthogonality and  
739 practical peak capacity considerations, *Journal of Chromatography A.* 1262 (2012) 148–  
740 159. <https://doi.org/10.1016/j.chroma.2012.09.028>.
- 741 [29] R.E. Murphy, M.R. Schure, J.P. Foley, Effect of Sampling Rate on Resolution in  
742 Comprehensive Two-Dimensional Liquid Chromatography, *Anal. Chem.* 70 (1998)  
743 1585–1594. <https://doi.org/10.1021/ac971184b>.
- 744 [30] K. Horie, H. Kimura, T. Ikegami, A. Iwatsuka, N. Saad, O. Fiehn, N. Tanaka,  
745 Calculating Optimal Modulation Periods to Maximize the Peak Capacity in Two-  
746 Dimensional HPLC, *Anal. Chem.* 79 (2007) 3764–3770.  
747 <https://doi.org/10.1021/ac062002t>.
- 748 [31] M. Sarrut, F. Rouvière, S. Heinisch, Theoretical and experimental comparison of one  
749 dimensional versus on-line comprehensive two dimensional liquid chromatography for  
750 optimized sub-hour separations of complex peptide samples, *Journal of*  
751 *Chromatography A.* 1498 (2017) 183–195.  
752 <https://doi.org/10.1016/j.chroma.2017.01.054>.
- 753 [32] C. Grivel, J.-L. Rocca, D. Guillaume, J.-L. Veuthey, S. Heinisch, Selection of suitable  
754 operating conditions to minimize the gradient equilibration time in the separation of  
755 drugs by Ultra-High-Pressure Liquid Chromatography with volatile (mass spectrometry-

- 756 compatible) buffers, *Journal of Chromatography A*. 1217 (2010) 459–472.  
757 <https://doi.org/10.1016/j.chroma.2009.11.059>.
- 758 [33] S.Chapel, S. Heinisch, F. Rouvière, A Theoretical and Practical Approach to Manage  
759 High Peak Capacity and Low Dilution in On-line Comprehensive Reversed-Phase LC ×  
760 Reversed-Phase LC: A Comparison with 1D-Reversed-Phase LC, *LC-GC Europe*  
761 (2020), vol 33, number s5, *Advances in UHPLC/HPLC*, 17-26.
- 762 [34] S.R. Groskreutz, S.G. Weber, Quantitative evaluation of models for solvent-based, on-  
763 column focusing in liquid chromatography, *Journal of Chromatography A*. 1409 (2015)  
764 116–124. <https://doi.org/10.1016/j.chroma.2015.07.038>.
- 765 [35] M. Bernardin, F. Bessueille-Barbier, A. Le Masle, C.-P. Lienemann, S. Heinisch,  
766 Suitable interface for coupling liquid chromatography to inductively coupled plasma-  
767 mass spectrometry for the analysis of organic matrices. 1 Theoretical and experimental  
768 considerations on solute dispersion, *Journal of Chromatography A*. 1565 (2018) 68–80.  
769 <https://doi.org/10.1016/j.chroma.2018.06.024>.  
770  
771

772

773 **Figure captions**

774

775 **Figure 1:** Schematic representation of the four interfaces for the four studied strategies: (a) Total  
776 breakthrough strategy (TBS); (b) Flow splitting strategy (FSS), (c) Make-up flow Strategy (MFS) and  
777 Active solvent modulation strategy (ASMS). The injected volumes are represented at the bottom of each  
778 scheme. Colours stand for the solvent strength (red for strong solvent, blue for weak solvent,  
779 purple for diluted solvent)

780 **Figure 2:** Schematic representation of the time repartition in <sup>2</sup>D with the four compared strategies  
781 (sampling time = 0.39 min): Total breakthrough (TBS), Flow splitting strategy (FSS), On-line dilution  
782 with make-up flow (MFS), and on-line dilution with ASM (ASMS).  $t_{loop}$ ,  $t_{D,instru}$ ,  $t_{iso}$ ,  $t_G$ ,  $t_{post}$ ,  $t_{eq}$  (Eqs. 3  
783 and 9) are represented by different colours. Experimental values are given in Table 1.

784 **Figure 3:** On-line HILIC x RPLC separations (2D-contour plots) of a tryptic digest of 6 proteins with (a)  
785 Total breakthrough strategy (TBS), (b) Flow splitting strategy (FSS), (c) Make-up flow Strategy (MFS),  
786 and (d) Active solvent modulation strategy (ASMS). The white dotted lines delimit the separation  
787 space. UV detection at 210 nm. Other conditions given in experimental section and in Table 1.

788 **Figure 4:** <sup>2</sup>D-separation of a strongly retained peptide (EIC 1622.5389) with four studied strategies  
789 used in on-line HILIC x RPLC: (a) Total breakthrough strategy (TBS); (b) Flow splitting strategy (FSS),  
790 (c) Make-up flow Strategy (MFS), and (d) Active solvent modulation strategy (ASMS). The  
791 characteristics of the retained peak are given in Table 4.

792 **Figure 5:** <sup>2</sup>D separation of a moderately retained peptide (EIC 588.3769) with four studied strategies  
793 used in on-line HILIC x RPLC: (a) Total breakthrough strategy (TBS); (b) Flow splitting strategy (FSS),  
794 (c) Make-up flow Strategy (MFS), and (d) Active solvent modulation strategy (ASMS). The  
795 characteristics of the retained peak are given in Table 4.

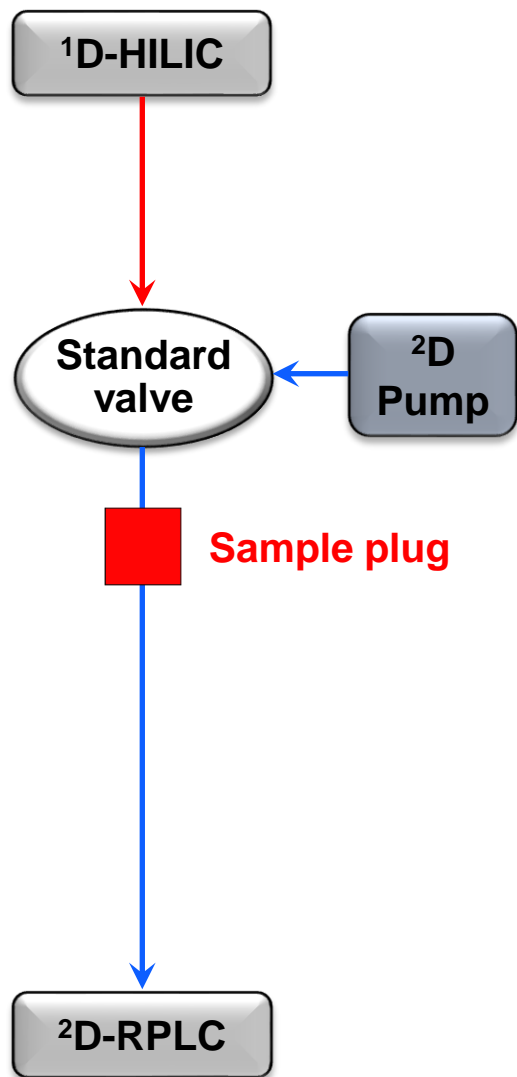
796 **Figure 6:** <sup>2</sup>D separation of a moderately retained peptide (EIC 723.3568) with four studied strategies  
797 used in on-line HILIC x RPLC: (a) Total breakthrough strategy (TBS); (b) Flow splitting strategy (FSS),  
798 (c) Make-up flow Strategy (MFS), and (d) Active solvent modulation strategy (ASMS). The  
799 characteristics of the retained peak are given in Table 4.

800 **Figure 7:** <sup>2</sup>D separation of a moderately retained peptide (EIC 779.4492) with four studied strategies  
801 used in on-line HILIC x RPLC: (a) Total breakthrough strategy (TBS); (b) Flow splitting strategy (FSS),  
802 (c) Make-up flow Strategy (MFS), and (d) Active solvent modulation strategy (ASMS). The  
803 characteristics of the retained peak are given in Table 4.

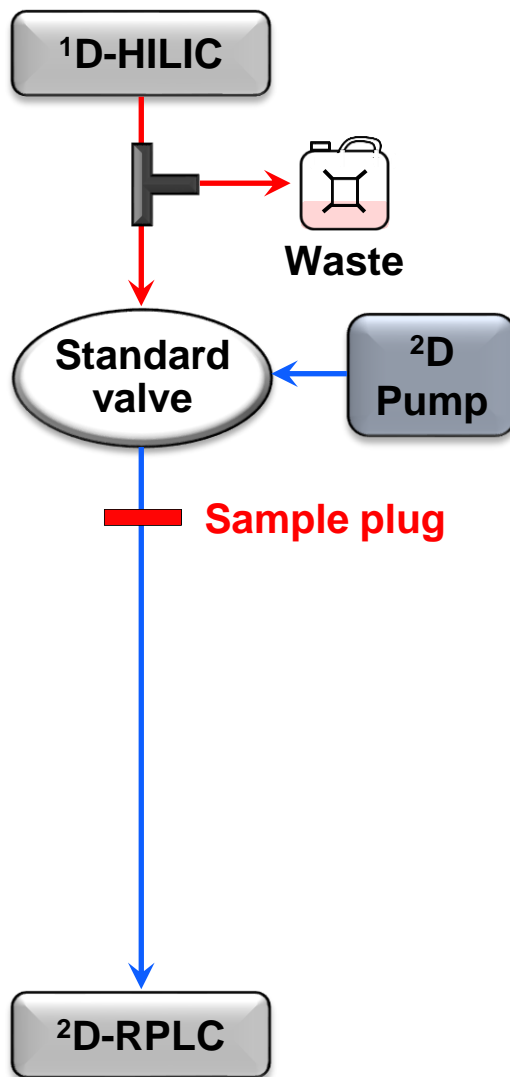
804 **Figure 8:** <sup>2</sup>D separation of a poorly retained peptide (EIC 830.4534) with four studied strategies used  
805 in on-line HILIC x RPLC: (a) Total breakthrough strategy (TBS); (b) Flow splitting strategy (FSS), (c)  
806 Make-up flow Strategy (MFS), and (d) Active solvent modulation strategy (ASMS). The characteristics  
807 of the retained peak are given in Table 4.

808

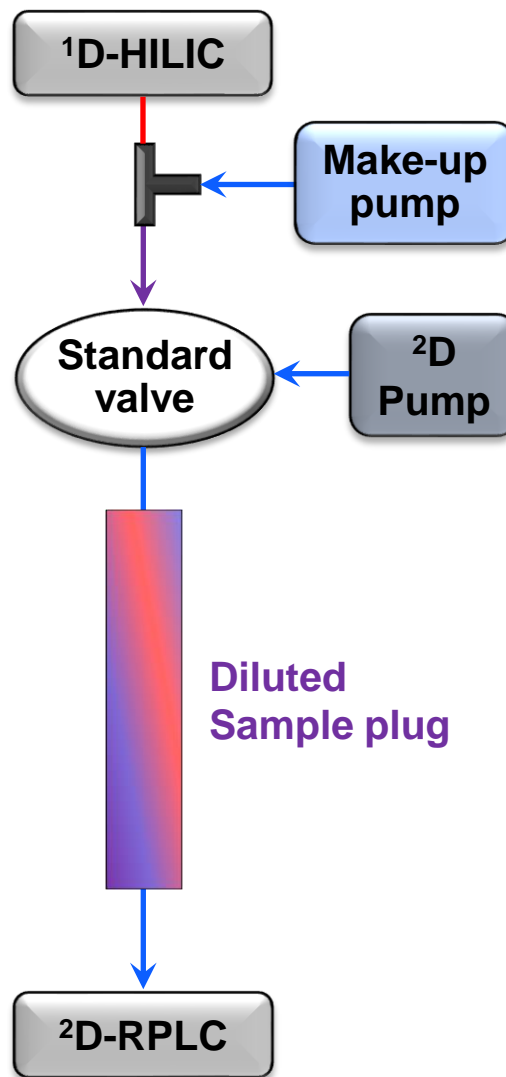
(a) TBS



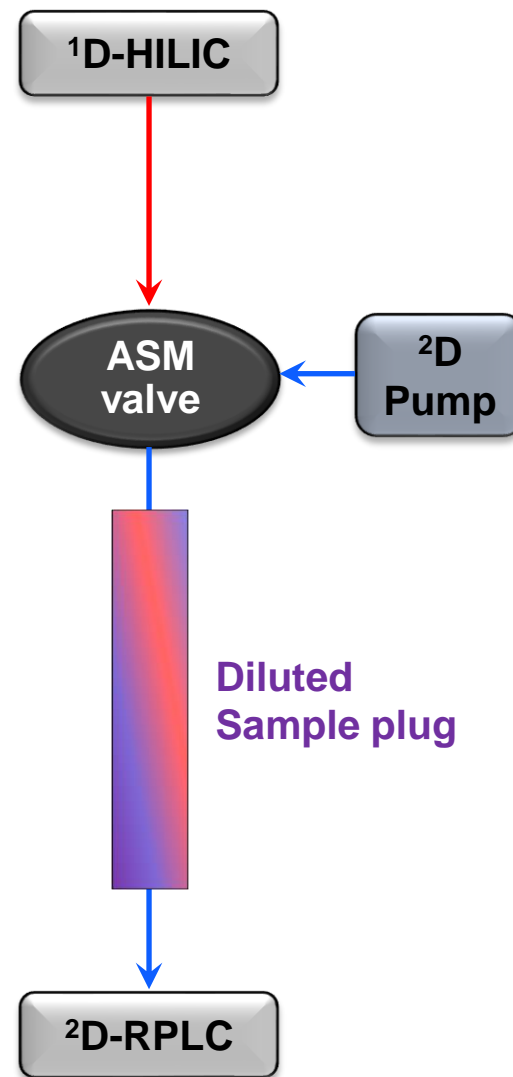
(b) FSS

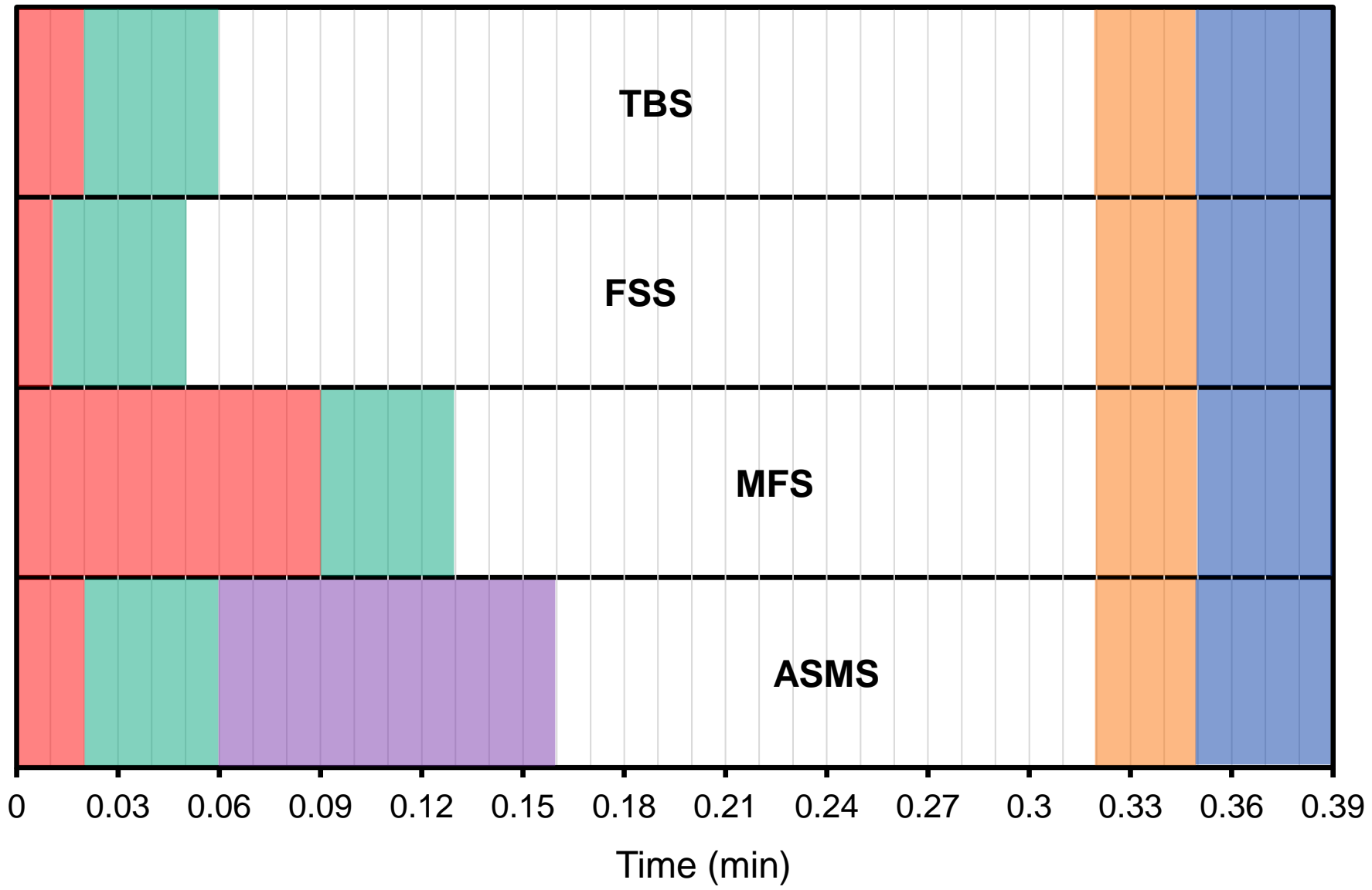


(c) MFS

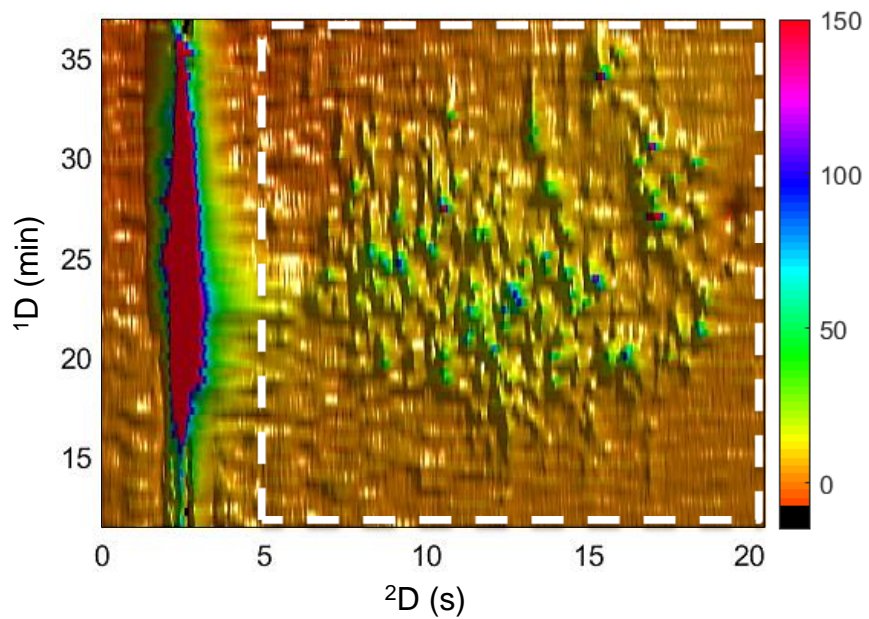


(d) ASMS

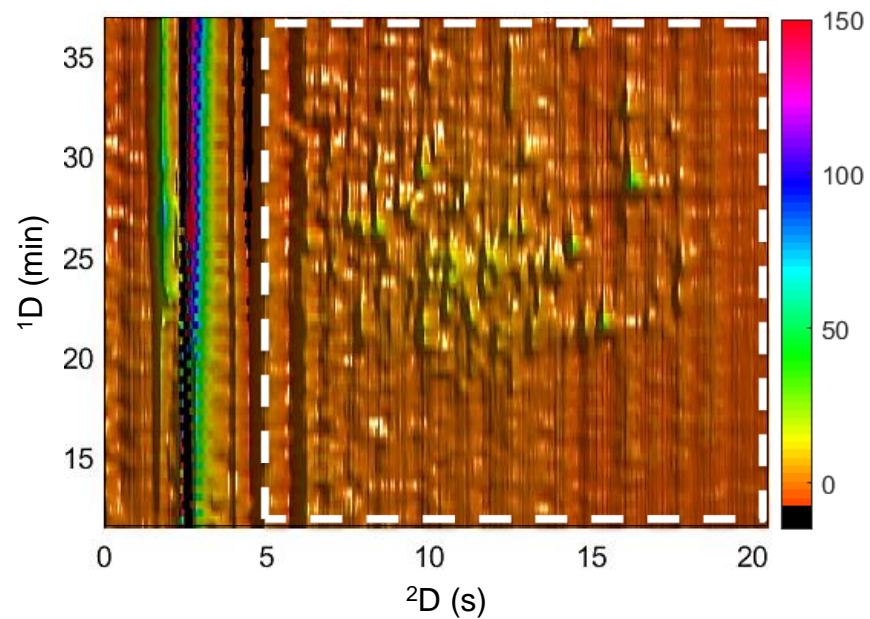




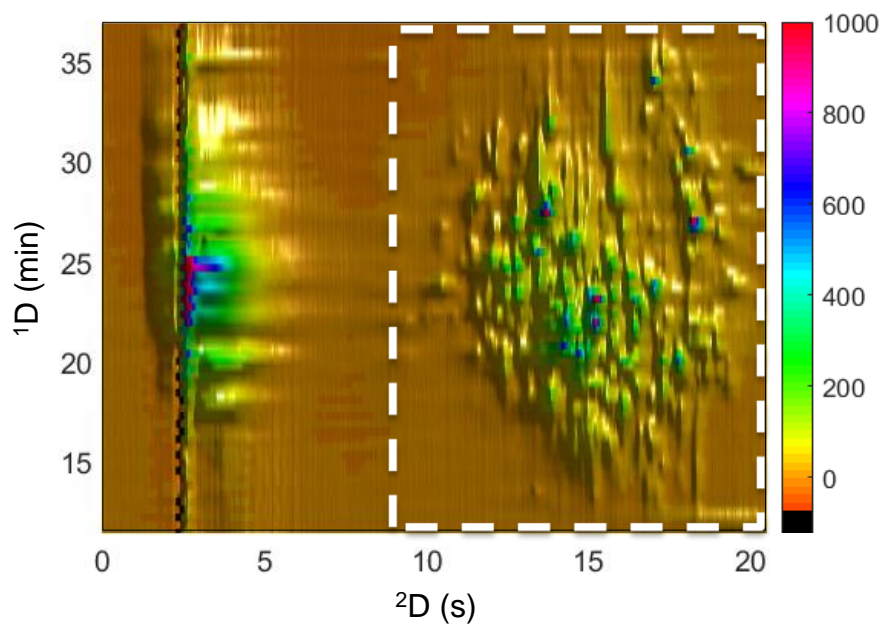
(a) TBS



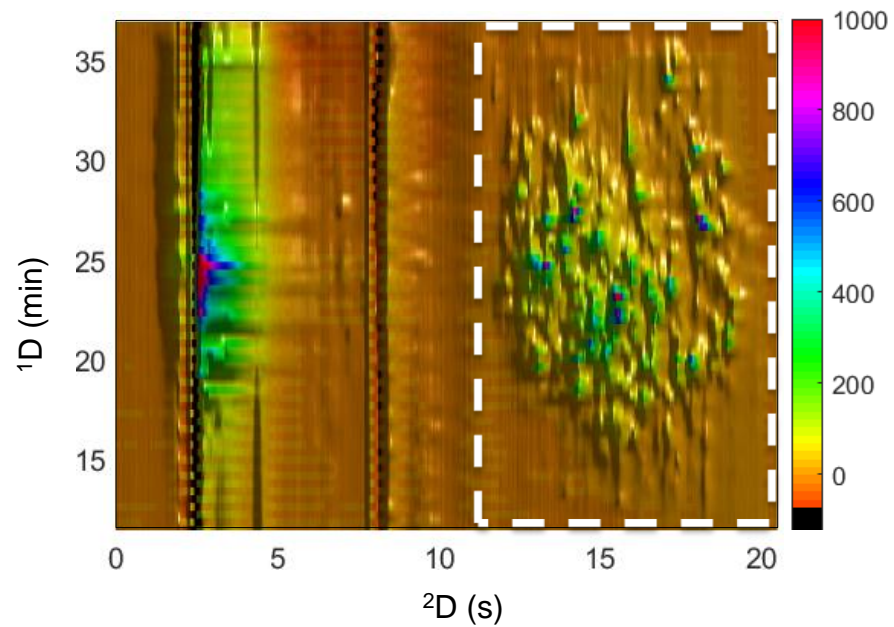
(b) FSS



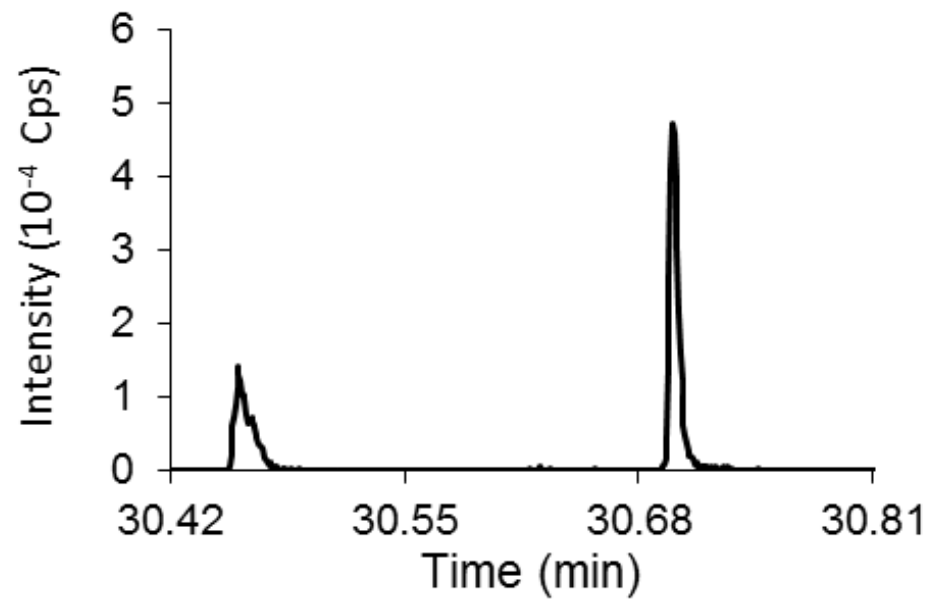
(c) MFS



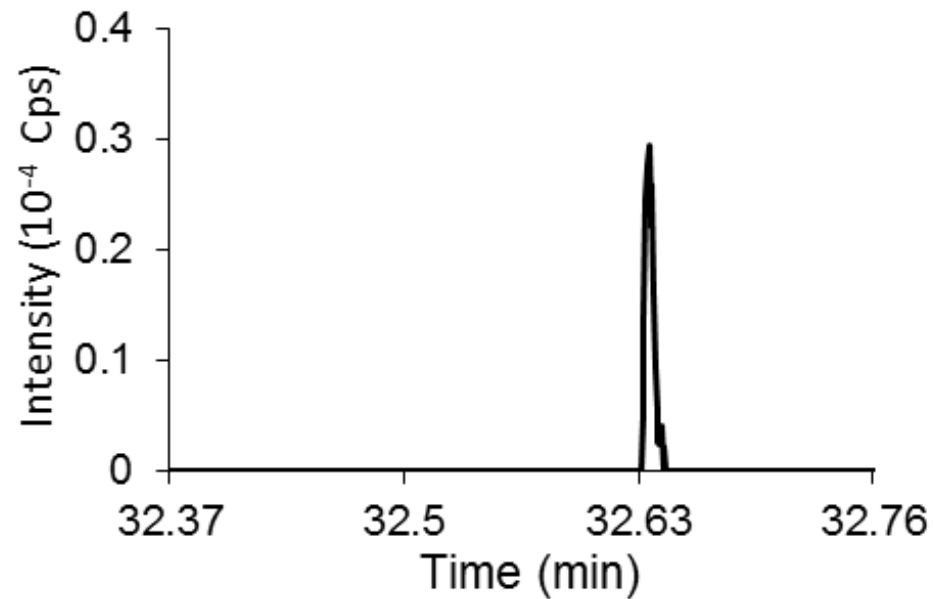
(d) ASMS



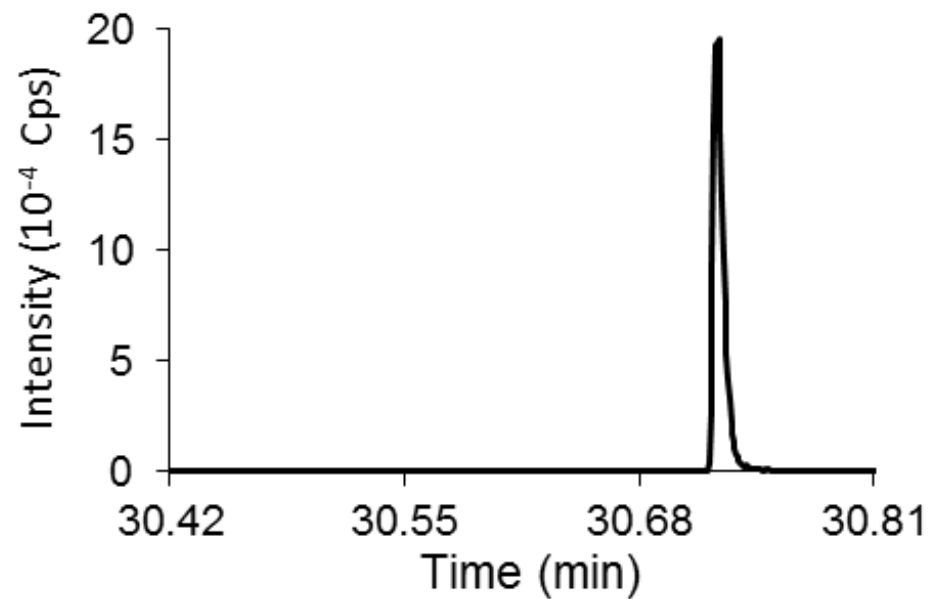
(a) TBS



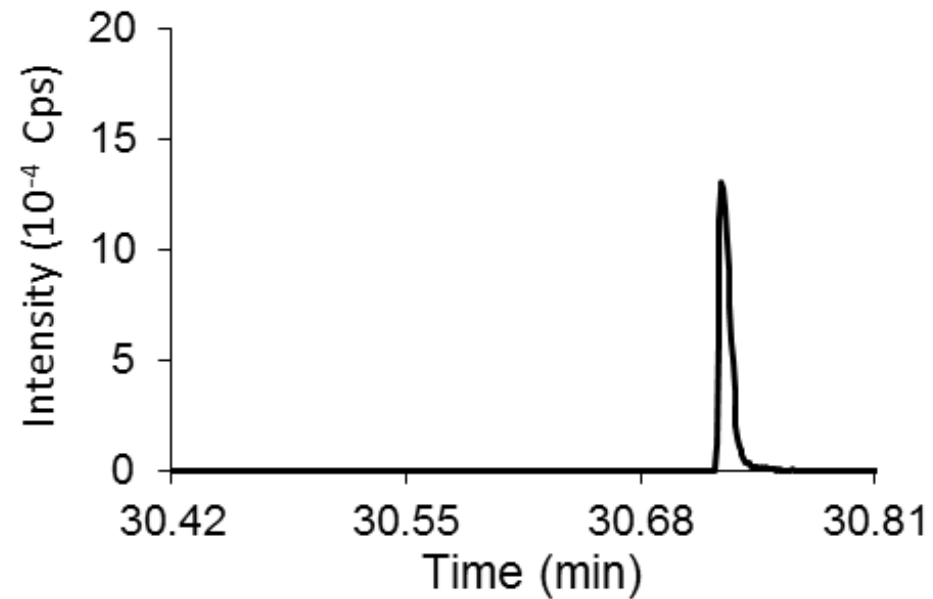
(b) FSS



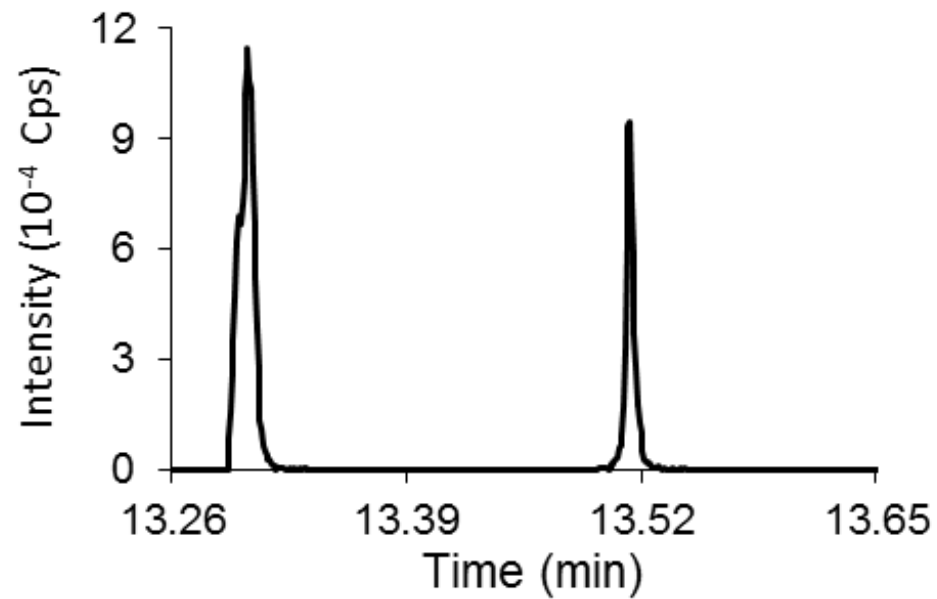
(c) MFS



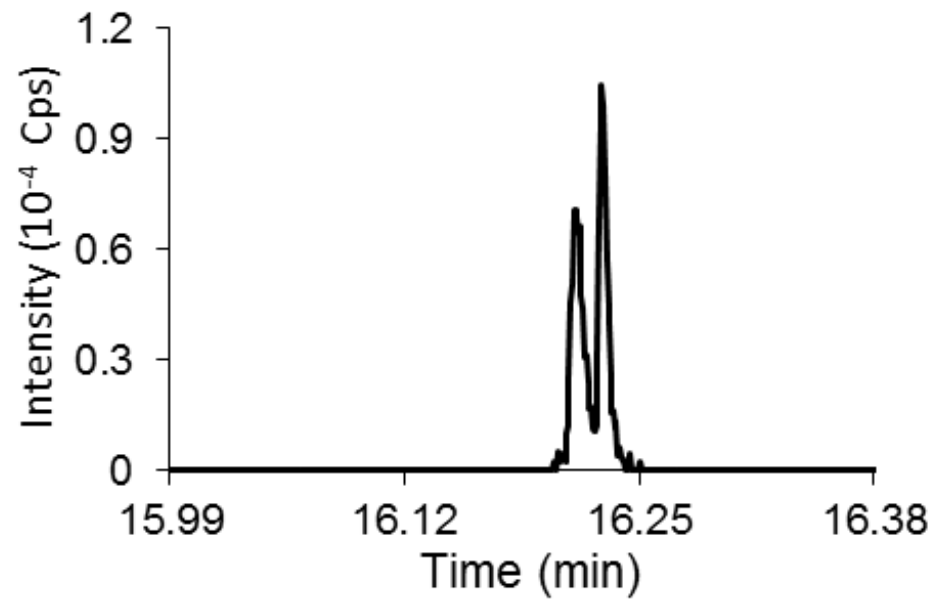
(d) ASMS



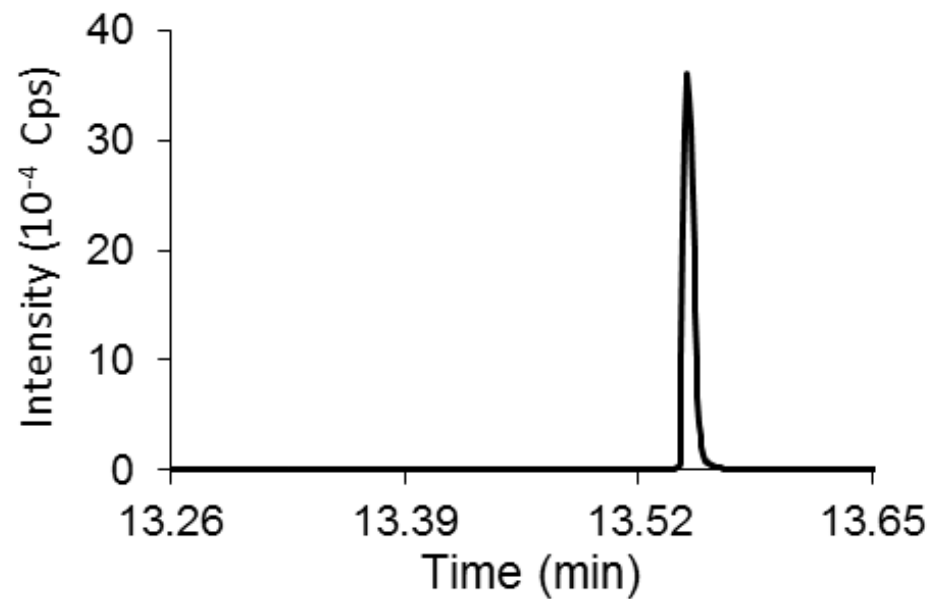
(a) TBS



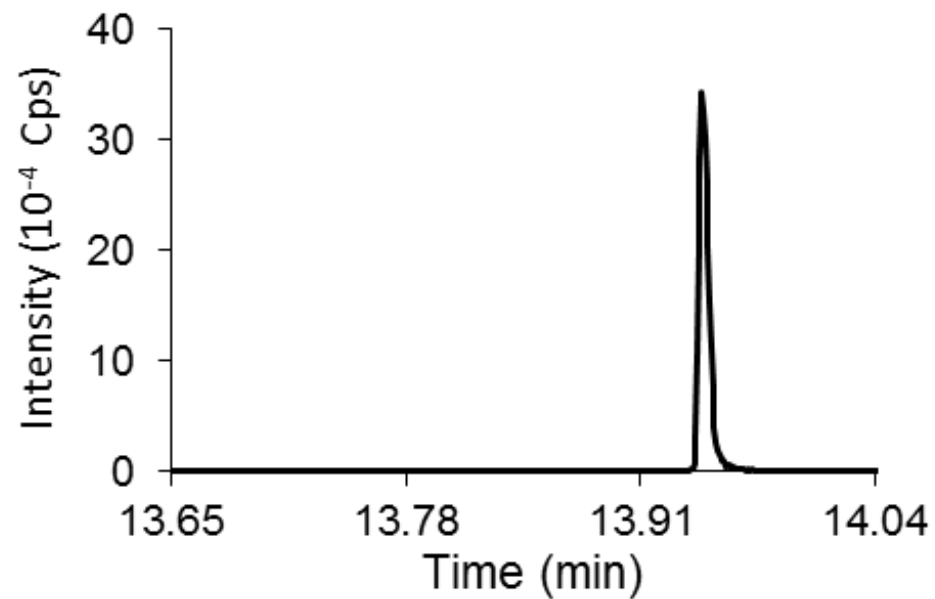
(b) FSS



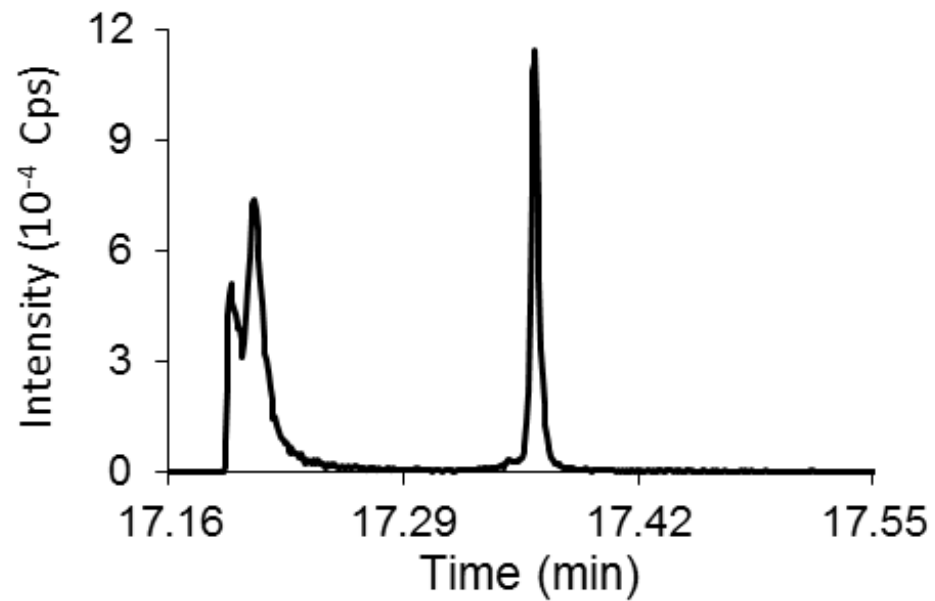
(c) MFS



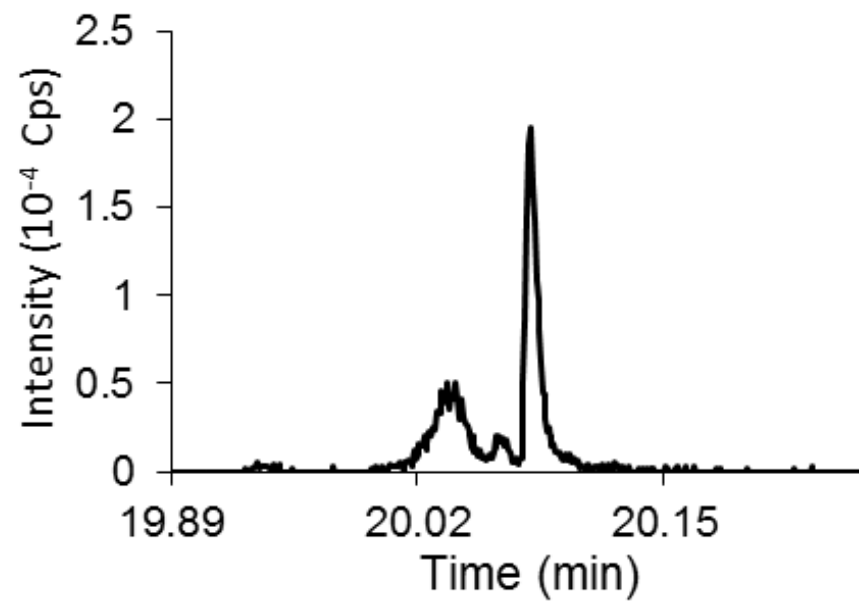
(d) ASMS



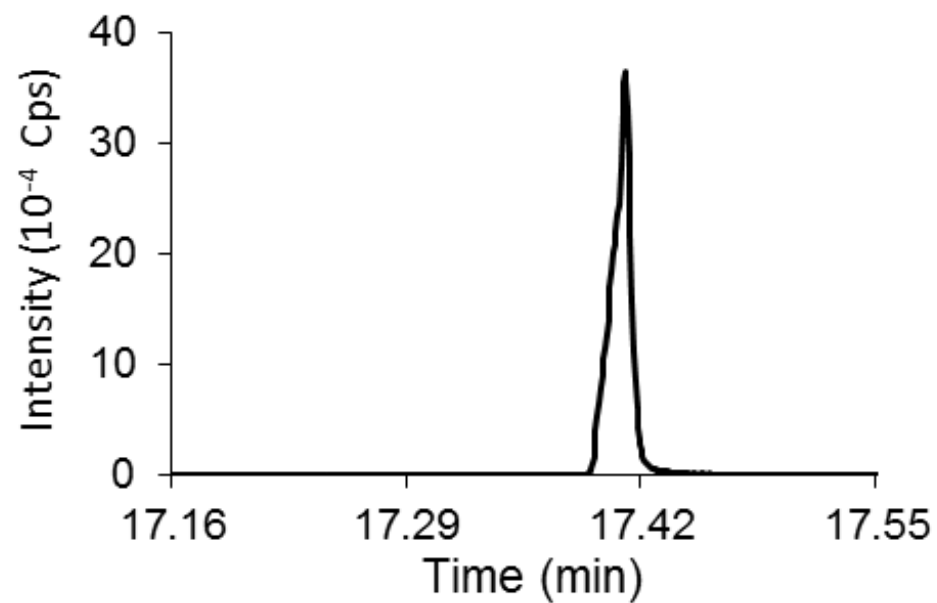
(a) TBS



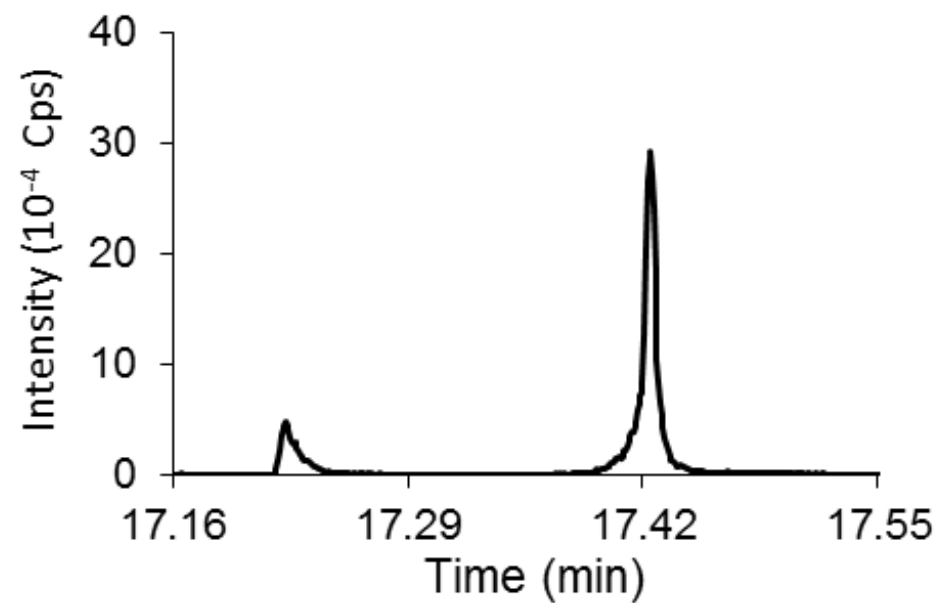
(b) FSS



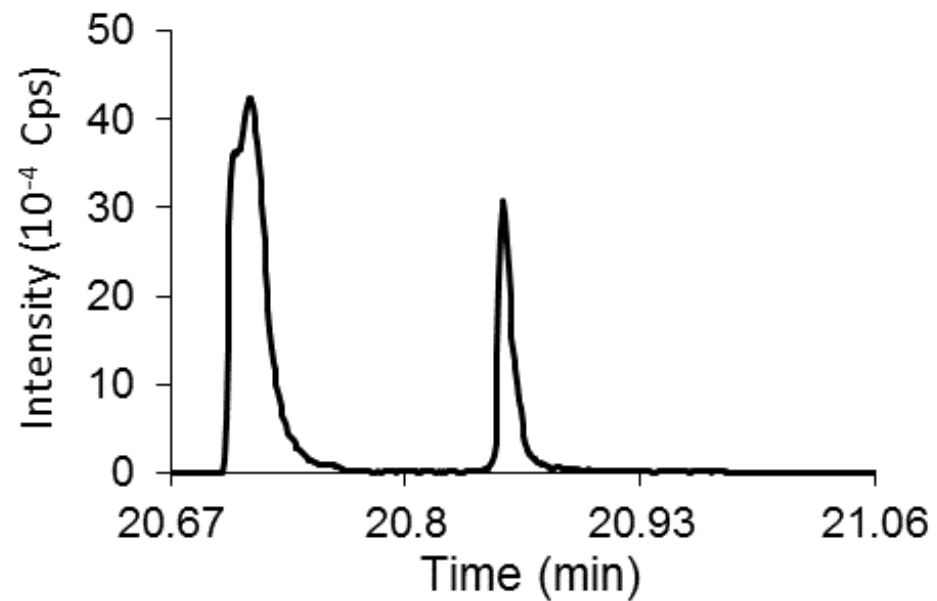
(c) MFS



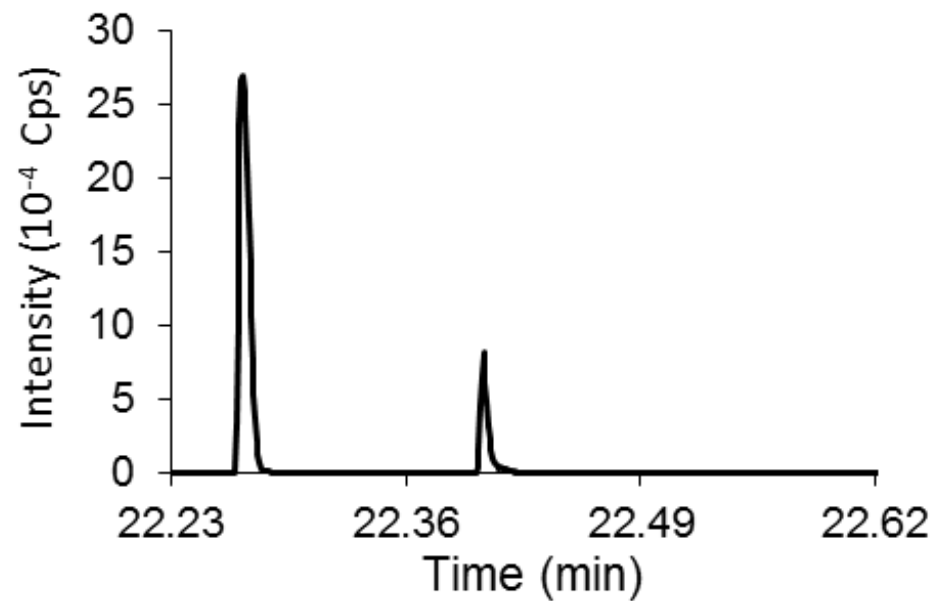
(d) ASMS



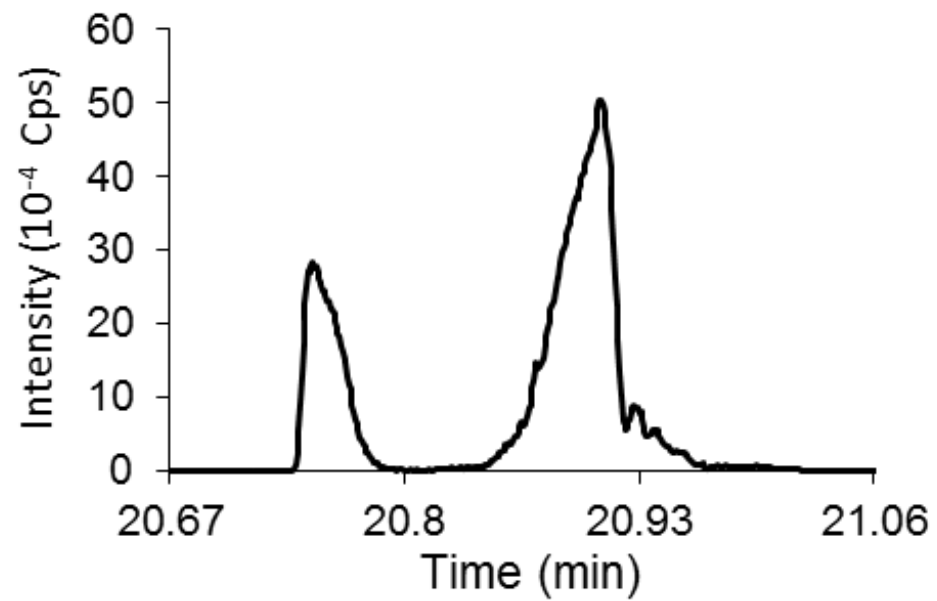
(a) TBS



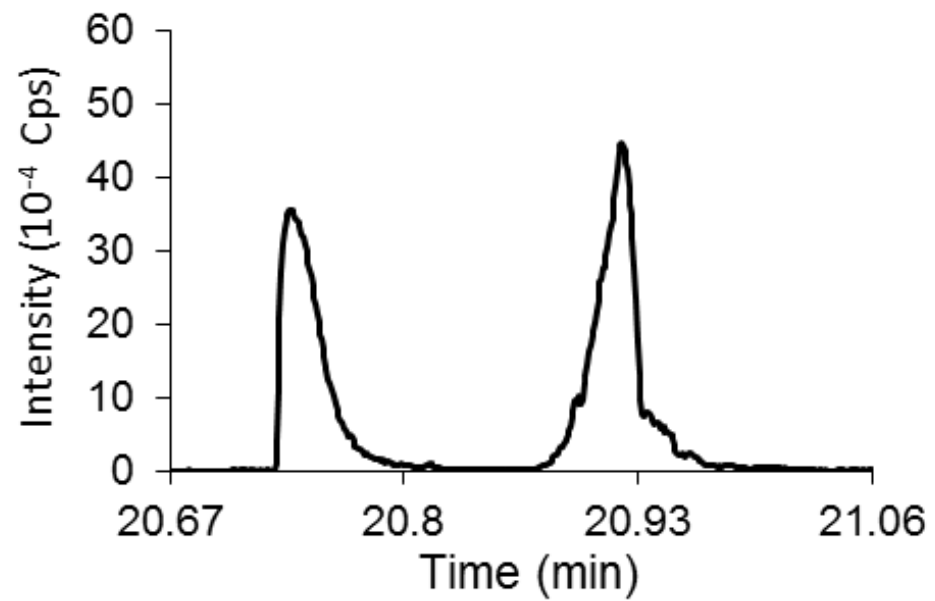
(b) FSS



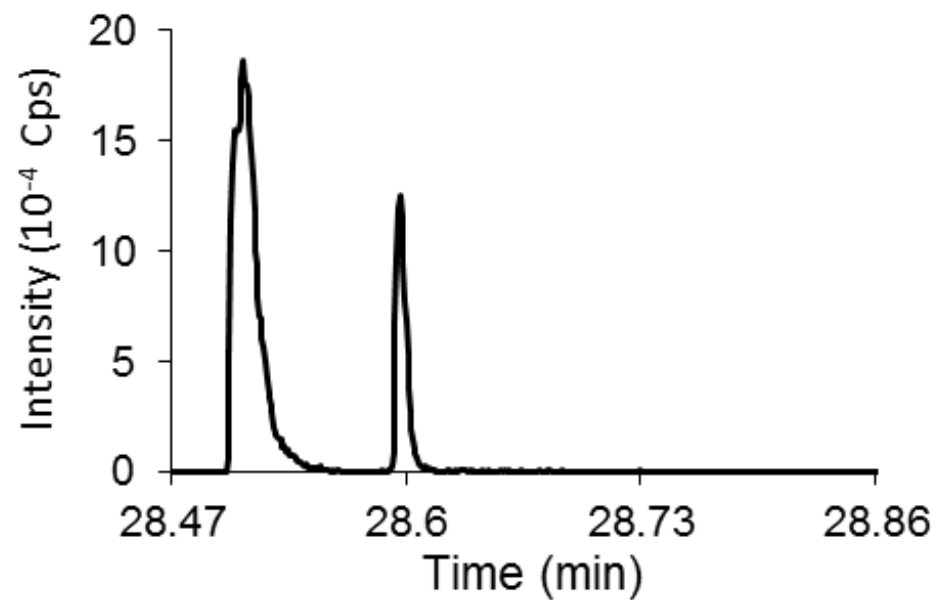
(c) MFS



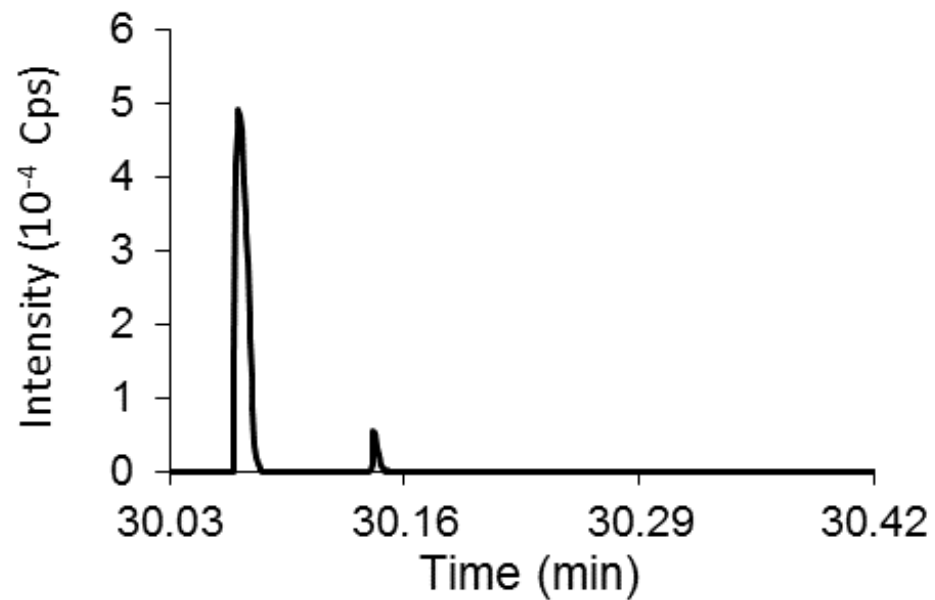
(d) ASMS



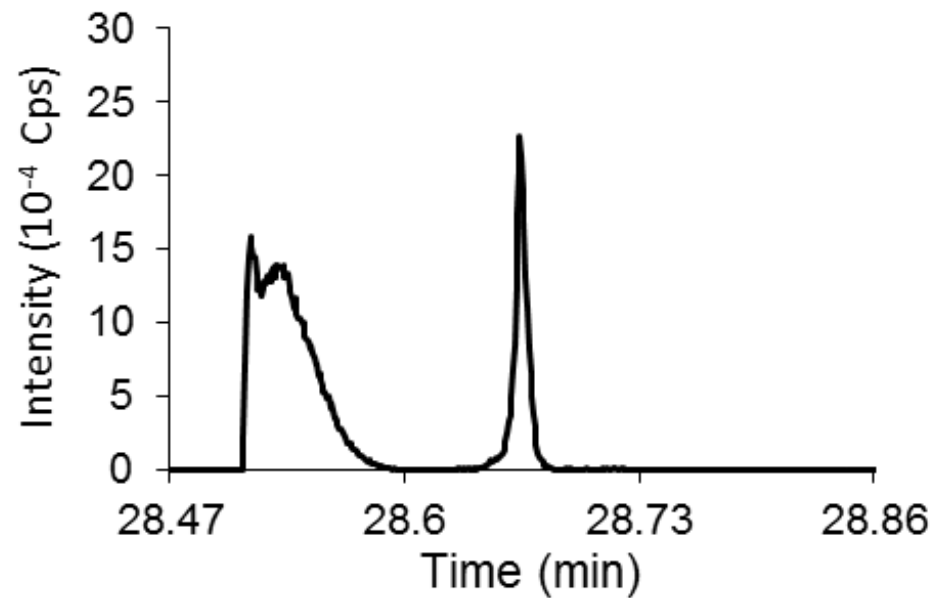
(a) TBS



(b) FSS



(c) MFS



(d) ASMS

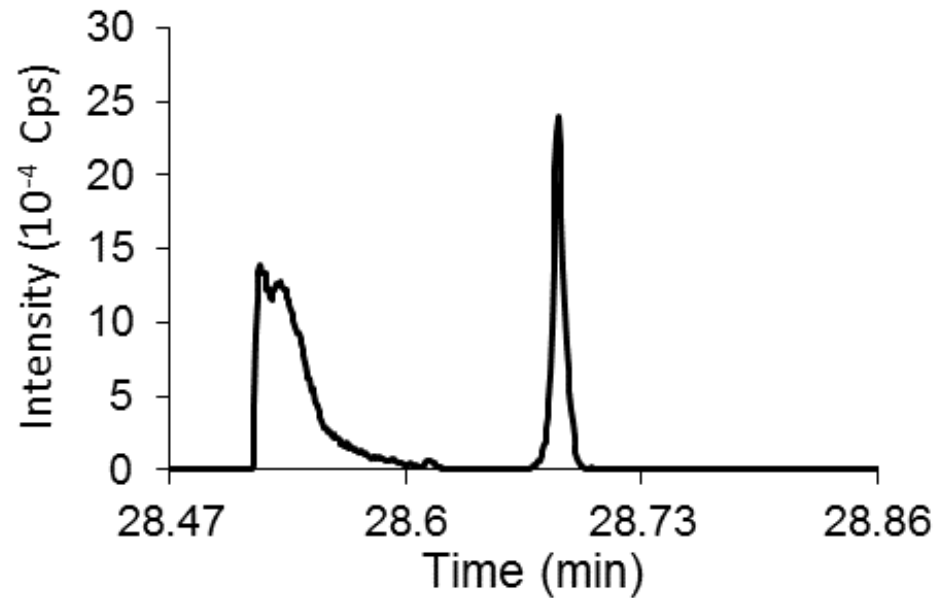


Table 1: Experimental interface conditions for the four compared strategies: total breakthrough strategy (TBS), flow splitting strategy (FSS), on-line dilution with make-up flow strategy (MFS), and on-line dilution with ASM strategy (ASMS). The different terms refer to Eqs. 3 to 9.  ${}^2F = 2000 \mu\text{L}/\text{min}$ ; sampling time = 0.39 min. The graphical representation of the time repartition is presented in Fig. 3.

	${}^1V_{\text{fraction}}$ ( $\mu\text{L}$ )	${}^1z_{\text{split}}$	${}^1z_{\text{dilution}}$	$V_{\text{loop}}$ ( $\mu\text{L}$ )	${}^2V_{\text{injection}}$ ( $\mu\text{L}$ )	${}^2t_{\text{loop}}$ (min)	${}^2t_{D,\text{instru}}$ (min)	${}^2t_{\text{iso}}$ (min)	${}^2t_G$ (min)	${}^2t_{\text{post}}$ (min)	${}^2t_{\text{eq}}$ (min)
TBS	19.5	1	1	40	19.5	0.02	0.04	0	0.26	0.03	0.04
FSS	1.95	10	1	20	1.95	0.01	0.04	0	0.27	0.03	0.04
MFS	97.5	1	5	180	97.5	0.09	0.04	0	0.19	0.03	0.04
ASMS	19.5	1	1	40	97.5	0.02	0.04	0.1	0.16	0.03	0.04

Table 2: Effective peak capacities ( $n_{2D,eff}$ ) and number of peptides identified compared to the expected number of peptides with the four compared strategies: Total Breakthrough strategy (TBS), Flow splitting strategy (FSS), On-line dilution with make-up flow strategy (MFS), and on-line dilution with ASM strategy (ASMS). Intermediate parameters for the peak capacity calculation (Eq. 1): ranges of elution times ( $\Delta t$ ) and average  $4\sigma$  peak widths ( $w_{4\sigma}$ ) measured with UV detection (210 nm). Other values required in Eq.1:  $\alpha = 0.673$  and  $\gamma = 1$ .

	<sup>1</sup> D		<sup>2</sup> D		$n_{2D,eff}$ (UV)	Number of peptides identified (%)
	<sup>1</sup> $\Delta T$ (min)	<sup>1</sup> $w_{4\sigma,UV}$ (min)	<sup>2</sup> $\Delta T$ (s)	<sup>2</sup> $w_{4\sigma,UV}$ (s)		
TBS	26	0.65	15.0	0.39	1100	99
FSS			15.6	0.46	970	86
MFS			11.0	0.41	770	99
ASMS			9.0	0.38	680	99

Table 3: Peak height ratios between different strategies for 39 relevant peaks well spread among the 2D-retention space. UV detection at 210 nm.

Peak #	$t_r$	m/z	Peak height ratio			
			TBS/FSS	MFS/TBS	ASMS/TBS	MFS/ASMS
1	21.1	1156.9329	22	1.1	3.5	0.3
2	21.4	1368.221	20	1.2	3.3	0.4
3	19.9	742.4514	4.1	6.0	5.8	1.0
4	26.9	1557.3634	9.6	3.1	2.6	1.2
5	30.4	1622.2051	21	3.7	3.3	1.1
6	19.9	1300.6981	5.3	6.8	6.8	1.0
7	23.8	864.9531	4.7	4.2	4.0	1.1
8	33.9	1057.5826	21	3.4	2.8	1.2
9	19.9	1231.5983	8.4	5.8	3.3	1.7
10	23.0	908.9567	6.1	6.9	6.4	1.1
11	26.1	680.9209	9.0	3.1	3.3	0.9
12	28.5	761.3974	7.6	4.8	6.2	0.8
13	30.8	460.2878	6.9	4.0	4.5	0.9
14	24.2	682.7068	6.6	3.5	4.5	0.8
15	25.0	748.3533	4.2	5.6	7.1	0.8
16	20.3	478.2555	6.3	7.1	5.6	1.3
17	22.6	482.772	8.0	13	13	1
18	23.0	692.4062	8.3	9.1	8.3	1.1
19	23.4	461.9383	7.4	4.8	4.1	1.2
20	26.1	756.4278	6.8	7.9	8.1	1.0
21	18.7	650.317	3.9	4.3	6.1	0.7
22	20.7	390.2289	5.8	8.5	7.4	1.1
23	19.9	890.3897	3.8	3.9	9.6	0.4
24	22.2	374.7234	4.0	7.1	6.0	1.2
25	23.4	500.8064	3.5	6.4	5.0	1.3
26	25.4	536.2919	6.7	7.2	7.1	1.0
27	26.1	488.287	7.7	2.7	2.3	1.2
28	27.3	584.817	7.5	6.9	5.6	1.2
29	28.5	627.982	12	5.7	5.4	1.1
30	32.0	547.319	15	5.7	5.4	1.1
31	19.5	513.2828	5.8	2.6	6.4	0.4
32	20.3	497.2036	7.9	1.6	3.8	0.4
33	24.6	424.5606	4.7	3.3	7.7	0.4
34	26.9	780.5013	8.8	4.5	6.8	0.7
35	24.6	636.3365	6.3	5.2	7.4	0.7
36	25.0	604.3474	5.3	3.0	3.1	1.0
37	32.0	415.7313	9.0	2.9	4.3	0.7
38	24.2	678.3842	3.9	2.0	2.6	0.8
39	18.7	1013.6022	8.4	5.4	4.8	1.1
<b>Average values</b>			<b>8.3</b>	<b>5.0</b>	<b>5.5</b>	<b>0.9</b>

TBS: Total breakthrough strategy

FSS: Flow splitting strategy

MFS: Make-up flow strategy

ASMS: on-line dilution with ASM strategy

$t_r$ : retention time in 1D

$m/z$  : mass-to-charge ratio

Table 4: Main characteristics of EICs shown in Figs.4 to 8 depending on the strategy used (TBS, FSS, MFS or ASMS).

Figure	m/z	Strategy	$t_r$ (min)	$C_{elution}^1$ (%) (Eq.2)	$C_{injection}^2$ (%) (Eq.7)	$t_r$ (min)	$C_{elution}^2$ (%) (Eq.2)	$\Delta C$ (%) (Eq.9)	$n_{2D,eff}$ (Eq.1)	Peak state <sup>(1)</sup>	$A_f$ (Eq.3)
4	1622.539	TBS	30.75	57	57	0.280	32	25	830	TB	1.6
		FSS	32.68	54	54	0.266	30	24	-	S	1.5
		MFS	30.77	57	12	0.302	32	-20	500	S	1.6
		ASMS	30.77	57	12	0.306	31	-19	400	S	2.1
5	588.377	TBS	13.56	86	86	0.253	28	58	750	TB	1.0
		FSS	16.28	81	81	0.240	26	55	-	D	1.5
		MFS	13.60	86	18	0.287	29	-11	550	S	1.4
		ASMS	13.99	85	18	0.293	28	-10	420	S	1.5
6	723.357	TBS	17.41	79	79	0.203	19	60	740	TB	1.1
		FSS	20.13	75	75	0.190	18	57	-	TS	-
		MFS	17.46	79	17	0.252	21	-4.2	260	D	0.8
		ASMS	17.47	79	17	0.263	19	-2.7	250	TS	0.8
7	779.449	TBS	20.90	73	73	0.184	16	57	570	TB	1.6
		FSS	22.45	71	71	0.173	15	56	720	TB	1.8
		MFS	20.96	73	15	0.240	18	-2.6	-	TS	-
		ASMS	20.97	73	15	0.252	16	-0.9	-	TS	-
8	830.453	TBS	28.65	60	60	0.127	6	54	590	TB	1.3
		FSS	30.19	58	58	0.113	5	52	-	TB	1.5
		MFS	28.71	60	13	0.193	7	5.7	370	TS	0.9
		ASMS	28.73	60	13	0.214	6	7.0	320	TS	1.1

<sup>(1)</sup> Peak state : TB: Total Breakthrough; S: single symmetrical retained peak; D: distortion and/or peak splitting; TS: transition step before Total Breakthrough;  $A_f$ : Asymmetry factor